Monodisperse Poly(triacetylene) Oligomers Extending from Monomer to Hexadecamer: Joint Experimental and Theoretical Investigation of Physical Properties

Rainer E. Martin,[a] Ulrich Gubler,[b] Jérôme Cornil,[c] Marina Balakina,[c] Corinne Boudon,[d] Christian Bosshard,[b] Jean-Paul Gisselbrecht,[d] François Diederich,*[a] Peter Günter,[b] Maurice Gross,[d] and Jean-Luc Brédas*[c, e]

Dedicated to Professor J. Barluenga on the occasion of his 60th birthday

Abstract: A series of monodisperse Et_3-Si-end-capped poly(triacetylene) (PTA) oligomers ranging from monomer to hexadecamer was prepared by a fast and efficient statistical deprotection–oxidative Hay oligomerization protocol. The PTA oligomers exhibit an increasingly deep-yellow color with lengthening of the π-conjugated backbone, feature excellent solubility in aprotic solvents, and exhibit melting points up to $>220\,^{\circ}C$ for the hexadecameric rod. This new dramatically extended oligo(enediyne) series now enables to investigate the evolution of the physico-chemical effects in PTAs beyond the linear $1/n$ versus property regime into the higher oligomer region where saturation becomes apparent. We report the results of joint experimental and theoretical studies, including analysis of the ^{13}C NMR spectra, evaluation of the linear (UV/Vis) and nonlinear [third-harmonic generation (THG) and degenerate four-wave mixing (DFWM)] optical properties, and characterization of the redox properties with cyclic and steady-state voltammetry. Up to the hexadecameric rod, an increasingly facile one-electron reduction step is observed, showing at the stage of the dodecamer, a leveling off tendency from the linear correlation between the inverse number of monomer units and the first reduction potential. The effective conjugation length (ECL) determined by means of UV/Vis spectroscopy revealed a π-electron-delocalization length of about $n = 10$ monomeric units, which corroborates well with the oligomeric length for which in the ^{13}C NMR spectrum $C(sp^2)$ and C(sp) resonances start to overlap. Third-harmonic generation (THG) and degenerate four-wave mixing (DFWM) measurements revealed for the second-order hyperpolarizability γ a power law increase $\gamma \cdot \alpha \cdot n^a$ for oligomers up to the octamer with exponential factors $a = 2.46 \pm 0.10$ and $a = 2.64 \pm 0.20$, respectively, followed by a smooth saturation around $n = 10$ repeating units. The power law coefficient a calculated with the help of the valence effective Hamiltonian (VEH) method combined to a sum-over-states (SOS) formalism corroborates well with the values found by both THG and DFWM experiments. Up to the PTA heptamer, INDO (intermediate neglect of differential overlap)-calculated gas-phase ionization potentials and electron affinities obey a linear relationship as a function of the inverse number of monomer units displaying a strong electron-hole symmetry. The onset of saturation for the electron affinity is calculated to occur around the octamer, in accordance with experimentally obtained results from electrochemical measurements.

Keywords: alkynes · conjugation · molecular wires · nonlinear optics · oligomers

[a] Prof. Dr. F. Diederich, Dr. R. E. Martin
Laboratorium für Organische Chemie, ETH-Zentrum
Universitätstrasse 16, 8092 Zürich (Switzerland)
Fax: (+41) 1 632 1109
E-mail: diederich@org.chem.ethz.ch

[b] Prof. Dr. P. Günter, PD Dr. C. Bosshard, Dipl.-Natw. U. Gubler
Nonlinear Optics Laboratory, Institute of Quantum Electronics
ETH-Hönggerberg, 8093 Zürich (Switzerland)

[c] Prof. Dr. J.-L. Brédas, Dr. M. Balakina, Dr. J. Cornil
Service de Chimie des Matériaux Nouveaux
Centre de Recherche en Électronique et Photonique Moléculaires
Université de Mons-Hainaut, Place du Parc, 20
7000 Mons (Belgium)

[d] Prof. Dr. M. Gross, Dr. C. Boudon, Dr. J.-P. Gisselbrecht
Laboratoire d'Electrochimie et de Chimie Physique du Corps Solide
Université Louis Pasteur, C.N.R.S.: U.M.R. no 7512
Faculté de Chimie, 1 et 4 rue Blaise Pascal
67008 Strasbourg (France)

[e] Prof. Dr. J.-L. Brédas
Department of Chemistry, The University of Arizona
1306 E. University Blvd, Tucson, AZ 85721-0041 (USA)

0947-6539/00/0619-3622 $ 17.50+.50/0

Introduction

Conjugated organic oligomers and polymers have stimulated an increasing interest over the last years owing to the fact that minor variations in their molecular structure can result in significant modifications of absorption, emission, or charge transport characteristics, which account directly for most of their interesting properties. In both, industry and academia, intense research activities aim to explore effects ranging from magnetism,[1] conductivity,[2] electronically stimulated light-emission (LEDs),[3] photoconductivity (photovoltaic cells)[4] to field-effect charge mobility (field-effect transistors, FETs),[5] nonlinear optical properties, and photorefractivity.[6] A significant advantage of organic materials compared with their inorganic counterparts lies in the potentially easy way they can be processed, for instance by spin coating, casting from solution, or ink jet printing; interestingly, the latter method allows patterning of large areas.[7] The design of high performance electroactive polymers needed for the construction of applicable devices usually requires a detailed characterization and careful analysis of their physical properties in order to allow for further optimization. However, systematic investigations of the physical properties of high molecular weight π-conjugated polymers are usually difficult to achieve since the solubility of such rigid rod-like polymers can be rather poor in common organic solvents. Furthermore, the formation of structural defects during polymer synthesis, workup, or subsequent material processing are usually inevitable, thus representing a further obstacle towards obtaining relevant physical data. In this respect, the study of soluble monodisperse oligomers with precisely defined length and constitution has emerged as an important tool to provide definite information on structural, electronic, and optical properties of the corresponding polydisperse polymeric analogs.[8, 9] The systematic study of such model compounds allows for a direct correlation between physical properties and chemical structures and enables the elaboration of useful and predictive structure–property relationships. The potential of monodisperse multinanometer-long π-conjugated rod-like oligomers to act as molecular wires in future molecular scale electronics and nanotechnological devices represents a further interest in this area.[10] This last aspect was a significant driving force into the research of monodisperse oligomers over the last years which culminated in the synthesis of various spectacular molecular architectures.[8, 9, 11–13]

In order to explore the chemistry and physics of poly(triacetylene)s [PTA, poly(*trans*-enediynes)] we recently reported the synthesis of a series of monodisperse Me_3Si-end-capped PTA oligomers ranging from the 0.96 nm long monomeric **1a** to the 4.61 nm long hexameric oligomer **1f**.[14] Their high solubility in a wide range of organic solvents, which is a direct consequence of the appended flexible $Me_2tBuSiOCH_2$ side chains, allowed the first comprehensive investigation of structure–property relationships in PTAs. On the basis of the results obtained for two polydisperse polymer samples **2a** and **2b**, which already showed saturation in their linear and third-order nonlinear optical properties and can thus be considered as data points for an infinite polymer chain, the effective conjugation length (ECL) in PTAs was estimated to comprise 7 to 10 monomer units or 42 to 60 C atoms.[14] The ECL[15, 16] is a measure for the number of repeat or monomer units that are required in a π-conjugated chain to render size-independent optical, redox, and other properties. This concept has been largely used for the theoretical and experimental understanding of the properties of various π-conjugated polymers. In order to access a detailed correlation between physical properties and lengthening of the π-conjugated backbone as well as a direct experimental determination of the ECL,[17–21] we have prepared the monodisperse PTA oligomer series **3a–g** which extends from a 6.07 nm long octameric (**3e**), to a 8.99 nm long dodecameric (**3f**), and a 11.9 nm long hexadecameric (**3g**) PTA rod.[22] This dramatically expanded oligo(*trans*-enediyne) series bridges the gap between the oligomer and polymer domains, allowing for a detailed investigation of the physical properties in PTAs up to the interesting saturation regime. The hexadecameric PTA rod **3g**, with its 16 double and 32 triple bonds between the terminal Si-atoms, represents the longest linear fully π-conjugated molecular wire without aromatic repeat units.[23]

We now report the synthesis of these molecular rods using a rapid and practical statistical deprotection-oxidative oligomerization protocol and describe the evolution of their linear optical, nonlinear optical, and electrochemical properties as a function of chain length. We have also calculated the gas-phase ionization potentials, electron affinities, lowest optically-allowed transition energies, and static γ values; the results are found to be in good agreement with the experimental data and provide a reliable framework for their interpretation. A detailed comparison between the physical properties of PTA oligomers and those of poly(acetylene) (PA) and poly(diacetylene) (PDA) chains comprising the same number of C atoms is also made.

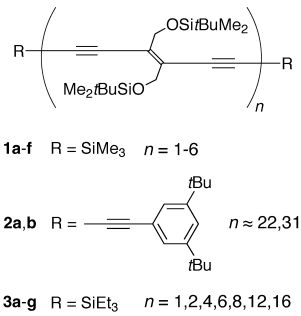

Results and Discussion

Synthesis of the Et_3Si-end-capped PTA oligomers: The general strategy for the synthesis of the higher monodisperse PTA oligomers **3c–g** relies on a statistical deprotection of the terminal triethylsilyl groups of suitable oligo(*trans*-enediyne) "macromonomers"; this generates a mixture of bis- and mono-deprotected oligomers (next to some unreacted starting material) which is then directly oligomerized under oxidative Hay conditions. This rapid and efficient synthesis protocol avoids isolation and tedious purification of the rather unstable unprotected alkyne intermediates. The synthesis of dimeric **3b**, which was utilized as a "macromonomer" in the first

  0947-6539/00/0619-3623 $ 17.50+.50/0

deprotection–oligomerization sequence giving access to tetrameric **3c** and hexameric **3d**, was achieved by statistical lithiation of *trans*-enediyne **4**[24, 25] with *n*BuLi in THF at −78 °C and subsequent trapping of the metallated species with Et_3SiCl (Scheme 1). Purification by column chromatography yielded the desired monosilylated **5** in 66% yield next to some unreacted **4** and bis-silylated monomer **3a**. However, monomer **3a** could conveniently be recycled upon treatment with NaOH in THF/CH_3OH 1:1 furnishing bis-deprotected **4** in nearly quantitative yield. Oxidative homocoupling of the asymmetrically substituted monomer **5** under Hay conditions using CuCl and *N*,*N*,*N*′,*N*′-tetramethylethylenediamine (TMEDA) in dry dichloromethane afforded dimeric **3b** in excellent yield of 97%.

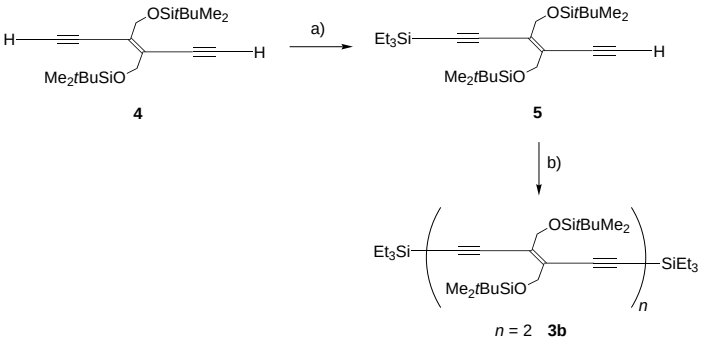

Scheme 1. Synthesis of "macromonomer" **3b** by statistical silylation of *trans*-enediyne **4** and oxidative dimerization of **5**. a) *n*BuLi, THF, −78 °C, 30 min, then $EtSi_3Cl$, 66%; b) CuCl, *N*,*N*,*N*′,*N*′-tetramethylethylenediamine (TMEDA), CH_2Cl_2, 4 Å molecular sieves, air, RT, 5 h, 97%.

Statistical deprotection of **3b** under kinetic control with NaOH in THF/MeOH 1:1 at RT afforded a mixture of monodeprotected **6a** and bis-deprotected **6b**, next to some unreacted starting material **3b** (Scheme 2). The progression of the protodesilylation was constantly monitored by thin-layer chromatography (silica gel, eluent: *n*hexane/AcOEt 40:1). Typical reaction times for the cleavage of the Et_3Si-groups in **3b** affording a mixture of **3b**, **6a**, and **6b**, which yields the best results in terms of isolable tetrameric **3c** and hexameric **3d**, are typically around 10 min. After quenching the reaction by addition of saturated aqueous NH_4Cl solution and extraction with CH_2Cl_2, the organic extracts were concentrated in vacuo to a volume of about 10 mL. Addition of CH_2Cl_2 (20 mL, containing 4 Å molecular sieves) and subsequent oxidative Hay oligomerization under an atmosphere of air, followed by workup and purification using preparative size-exclusion chromatography (SEC, 5 × 180 cm glass column filled with Bio-Rad Bio-Beads SX-1, CH_2Cl_2), provided predominantly tetrameric **3c** in about 20% yield next to minor amounts of hexameric **3d** (≈5% yield) and traces of unseparable polymers (<5%). Re-isolated dimeric **3b** (≈70% yield) was then used in the next deprotection–oligomerization cycle, thus making this route overall very efficient.

In a similar procedure, based on tetrameric **3c**, statistical deprotection produced a mixture of **3c**, mono-deprotected **7a**, and bis-deprotected **7b**, which upon oligomerization afforded monodisperse octameric **3e** (20%), dodecameric **3f** (10%), and hexadecameric **3g** (5%) as the main products besides recovered **3c** (50%, Scheme 2). In order to allow for a complete conversion of the free diethynyl species **7b**, the reaction conditions needed to be slightly adapted, and the oligomerization was then performed in toluene under reflux in an atmosphere of dry O_2. Purification of all oligomers up to dodecameric **3f** was performed by preparative SEC as described above, whereas the isolation of pure hexadecameric **3g** required preparative SEC on a commercial TosoHaas TSKgel G3000 HR (5 μm, 2.15 × 60 cm) column. In all cases, the purity of the fractions was examined by analytical SEC since this technique can detect levels of impurity down to approximately 5%. Final purification of the oligomers involves in all cases precipitation from MeOH and subsequent isolation of the solid material by centrifugation. An improved synthesis of hexadecameric **3g** (20% yield) was accomplished employing octameric **3e** as the "macromonomer" in the statistical deprotection–oligomerization sequence. As a direct consequence of the larger difference in molecular weights of the oligomers formed in this conversion, the separation and purification of **3g** by SEC was significantly improved.

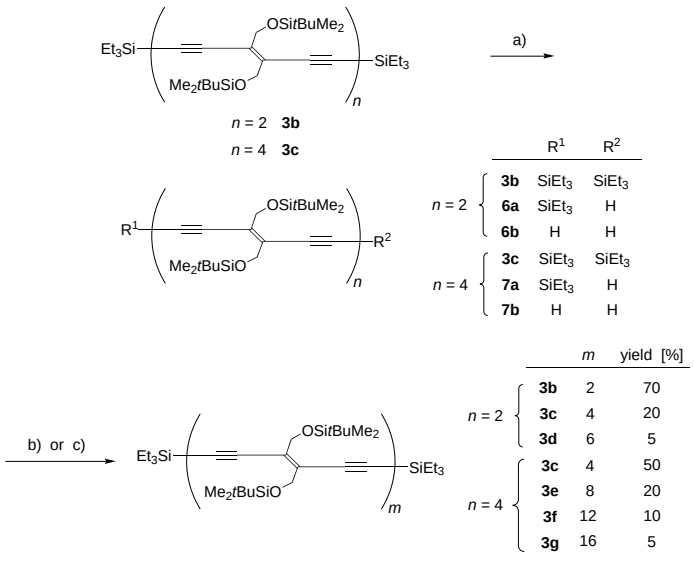

Scheme 2. Synthesis of PTA oligomers **3c–g** by statistical deprotection–oligomerization sequences. a) NaOH, THF/MeOH 1:1, 20 °C, 20 min; b) (for $n = 2$): CuCl, *N*,*N*,*N*′,*N*′-tetramethylethylenediamine (TMEDA), CH_2Cl_2, 4 Å molecular sieves, air, RT, 2 h; c) (for $n = 4$): CuCl, TMEDA, toluene, 4 Å molecular sieves dry O_2 atmosphere, reflux, 1 h.

As already observed for the oligomer series **1a–f** bearing Me_3Si-end groups, compounds **3a–g** exhibit an increasingly deep yellow color with lengthening of the π-conjugated backbone. All oligomers, including hexadecameric **3g**, feature excellent solubility in aprotic solvents such as toluene and CH_2Cl_2, but are insoluble in protic solvents. The pure oligomers are highly stable for months under standard laboratory conditions, with melting points (m.p.) going up to >220 °C for hexadecameric **3g** (Table 1).

The new oligomers were fully characterized by melting points, ^1H and ^{13}C NMR, UV/Vis, FT-IR, Raman spectra, MALDI-TOF-MS, and elemental analysis. In particular, mass spectrometry measurements using either mixtures of 2′,4′,6′-trihydroxyacetophenone (THA)/ammonium hydrogencitrate (AHC) or 3-(3-indolyl)acrylic acid (IAA) as matrices were of

0947-6539/00/0619-3624 $ 17.50+.50/0 *Chem. Eur. J.* **2000**, *6*, No. 19

Table 1. Estimated rod length, thermal, and optical properties of the Et_3Si-end-capped PTA oligomers **3a–g**.

Compound	n	l [Å][a]	M.p. [°C][b]	λ_{max} [nm][c]	E_{max} [eV]	ε [$M^{-1}cm^{-1}$][d]	E_g [eV][e]
3a	1	9.6	–	299.6 ± 0.1	4.14	21400	4.00
3b	2	16.9	69	379.4 ± 0.1	3.27	26200	3.13
3c	4	31.5	151	439.2 ± 0.2	2.82	37200	2.66
3d	6	46.1	183	463.7 ± 0.8	2.67	36500	2.55
3e	8	60.7	202	468.1 ± 0.8	2.65	55700	2.50
3f	12	89.9	219	471.2 ± 0.6	2.63	85900	2.48
3g	16	119.1	> 220	471.8 ± 0.6	2.63	112000	2.48

[a] Length estimated from terminal Si to Si atom by molecular mechanics calculations as in ref.[14]. It should be noted that any molecular rod of this type has a finite bending modulus and will therefore exhibit normal modes of vibration in thermal equilibrium and thus might be considered as being straight only on time average. [b] Uncorrected. [c] Longest-wavelength absorption maximum in $CHCl_3$ at RT, obtained by deconvolution of the absorption spectra, see [14]. [d] Molar extinction coefficient. [e] Solution optical band gap, estimated from the onset of absorption.

high diagnostic value owing to the fact that they displayed for oligomers **3b–g** the molecular ion ($[M+Na]^+$) as the most intensive signal. For hexadecameric rod **3g**, only the molecular ion ($[M+Na]^+$) at $m/z = 6056$ Da (6055.5 Da calculated for the most abundant isotope in the molecular ion cluster, $^{12}C_{329}{}^{13}C_3H_{574}O_{32}{}^{28}Si_{31}{}^{29}Si_2{}^{30}Si^{23}Na^+$) is observed and no trace of the octameric starting material **3e**, thus clearly indicating the purity of the hexadecamer.[22]

The excellent solubilities of the oligomers, which can be largely ascribed to the laterally appended $Me_2tBuSiOCH_2$ groups, allowed full characterization of the molecular PTA rods by ^1H and ^{13}C NMR spectroscopy. Up to octameric **3e**, all resonances for the C atoms of the conjugated backbone are clearly separated in the ^{13}C NMR spectra, showing for **3e** 8 C(sp^2) resonances between $\delta = 129$ and 133, 2 outer alkyne C(sp) resonances at $\delta = 102$ and 107, and 14 interior alkyne C(sp) resonances between $\delta = 81$ and 88. In contrast, the C(sp^2) and inner alkyne C(sp) resonances in dodecameric **3f** and hexadecameric **3g** displayed severe overlap in the expected spectral regions. It is of interest to notice that the ^{13}C NMR resonance overlap starts at an oligomer length (between the 8-mer **3e** and 12-mer **3f**) which corresponds well to the ECL of PTAs estimated from UV/Vis spectroscopy, nonlinear optical measurements, and Raman spectroscopy,[22] although there is no direct correlation between these two physical methods (vide infra). Both NMR and IR spectra do not provide any indication for photochemical *trans* → *cis* isomerization of the molecular rods **3a–g**; this suggests that the oligomers are present in the all-*trans* configuration. These results are in agreement with previous work where photochemically induced isomerizations were only observed for donor and/or acceptor substituted, arylated 1,2-diethynylethenes and tetraethynylethenes.[26] In addition, X-ray crystal structure analyses of PTA oligomers clearly showed a preference of the planar backbones for the *s-trans* conformation (orientation of two double bonds with respect to the connecting −C≡C−C≡C− fragment) since this geometry best accommodates the bulky lateral silyl groups.[27]

Electrochemical behavior of the PTA oligomers: The redox characteristics of the Et_3Si-end-capped oligomer series **3b–g** were studied by cyclic (CV) and steady-state voltammetry (SSV) in CH_2Cl_2 and 0.1 M nBu_4NPF_6 as supporting electrolyte (Table 2). In accord with the electrochemical behavior and potentials observed previously for compounds **1a–f**,[14] all Et_3Si-end-capped oligomers, except hexadecamer **3g**, were reversibly reduced in a one-electron step. Interestingly, only octameric **3e** and dodecameric **3f** could be oxidized at +1.20 V versus Fc/Fc^+ and +1.13 V versus Fc/Fc^+, respectively, despite the fact that in the Me_3Si-end-capped PTA series **1a–f** oxidation events were already observed for **1b–f**.[14] A poorly resolved peak potential was obtained for the higher Et_3Si-end-capped species **3g** from both cyclic and steady-state voltammetry. In agreement with measurements on the earlier PTA oligomer series **1a–f**, the new Et_3Si-end-capped oligomers **3b–g** revealed an increasingly facile first reduction upon elongation of the π-conjugated chain. Plotting the first reduction potentials of series **3b–g** versus $1/n$ gives a straight linear correlation up to hexamer **3d**, followed by an onset of saturation for octamer **3e** and dodecamer **3f** (Figure 1). Interestingly, the first reduction potential of hexadecamer **3g** slightly deviates from the expected saturation value. This might be a consequence of the rather high uncertainty for this reduction potential, owing to the poor resolution of the reduction wave and its irreversible behavior. Taking the average value of the data points obtained for **3e**

Table 2. Electrochemical data for Et_3Si-end-capped PTA oligomers **3b–g**.

Compound	n	Cyclic voltammetry			Steady-state voltammetry	
		E'^0[a]	ΔE_p [mV][b]	E_{pa}[c]	$E_{1/2}$[d]	slope [mV][e]
3b	2	−2.10	102	–	−2.11	73
3c	4	−1.76	95	–	−1.77	55
		−1.90	63	–	−1.90	70
3d	6	−1.71	90	–	−1.72	70
3e	8	−1.69	80	+1.20	−1.70	65
		–	–	–	−2.25	125
		–	–	–	+1.20	110
3f	12	−1.72	160	–	−1.69	95
		–	–	–	+1.13	85
3g	16	−1.79[f,g]	–	–	−1.76	–

[a] V vs. Fc/Fc^+, redox potentials observed in CH_2Cl_2+0.1 M nBu_4NPF_6, scan rate $\nu = 100$ mV s^{-1}, formal redox potential $E'^0 = (E_{pa}+E_{pc})$. [b] $\Delta E_p = E_{ox} - E_{red}$, where subscripts ox and red refer to the conjugated oxidation and reduction steps, respectively. [c] Peak potential E_{pa} for irreversible oxidation. [d] V vs. Fc/Fc^+, rotating disk electrode in CH_2Cl_2+0.1 M nBu_4NPF_6. [e] Logarithmic analysis of the wave obtained by plotting E vs. $\log[I/I_{im} - I)]$. [f] Irreversible electron transfer. [g] Peak potential poorly resolved.

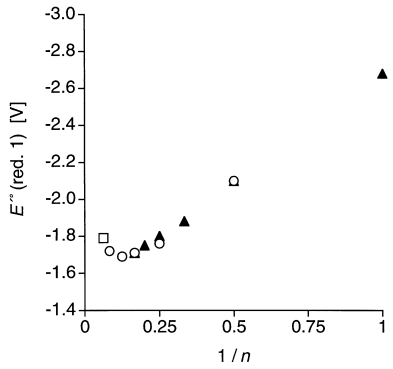

Figure 1. Evolution of the first reversible reduction potential of Me_3Si-end-capped PTA oligomers **1a–f** (▲), higher Et_3Si-end-capped PTA oligomers **3b–f** (○), and hexadecamer **3g** (□) obtained by cyclic voltammetry recorded in CH_2Cl_2 (0.1M nBu_4NPF_6, V vs. Fc/Fc^+). The hexadecamer **3g** revealed a poorly resolved irreversible peak potential.

and **3f**, the first reduction potential of an infinite PTA chain is estimated to $E_{red} = -1.70$ V versus Fc/Fc^+. In addition, the crossing between the linear regression through the data obtained for oligomers **3b–d** and the horizontal saturation line of **3e**,**f** (intercepting the *y* axis at −1.70 V) yields an ECL of about $n = 10$ monomer units, which is in good agreement with the results obtained from UV/Vis spectroscopy, nonlinear optical measurements (vide infra), and Raman spectroscopy.[22] This result provides evidence that the wavefunction associated to the generated charged species (i.e., polarons) extends approximately over 10 monomer units or 60 C π-centers. It has to be noted that a plot of the first reduction potentials obtained from steady-state voltammetry versus the inverse number of oligomer units shows an even more pronounced saturation behavior for **3e** and **3f**, with the value measured for hexadecamer **3g** lying closer to the expected curve than in the case of the cyclic voltammetry data.

The difference between the oxidation and reduction potentials obtained from steady-state voltammetry for dodecamer **3f** yields an electrochemically derived HOMO–LUMO gap of $\Delta E = 2.82$ eV, which matches the value of $\Delta E = 2.82$ eV corresponding to the most-intensive absorption band in the UV/Vis spectrum. However, the deconvolution of the absorption spectrum[14] of **3f** yields a slightly lower value for λ_{max} ($\Delta E = 2.63$ eV). The difference between the electrochemical HOMO–LUMO gap and the energy of the 0–0 absorption band in the UV/Vis spectrum is an indication of the binding energy of the exciton generated in the lowest optically-allowed transition, which is typically on the order of a few tenths of an eV.[28]

The observed linear behavior of the first reduction potentials versus $1/n$ for shorter oligomer lengths in the present series of monodisperse PTA oligomers is not without precedence. Similar observations for the evolution of redox potentials upon extension of the π-conjugated backbone were reported, for example for oligo(α-thiophene)s by Bäuerle,[29] for oligo(α-thiophene vinylene) oligomers by the group of Roncali,[30] or by Müllen and co-workers[31] for a series of oligo(*p*-phenylene vinylene)s.

Linear optical properties of the PTA oligomers: The UV/Vis spectra of the Et_3Si-end-capped oligomers were recorded in $CHCl_3$ solutions at RT and are depicted in Figure 2. For the shorter representatives up to octameric **3e**, the deconvoluted[14] longest-wavelength absorption maximum λ_{max} shifts bathochromically with increasing chain length, whereas for the higher oligomers this shift vanishes (Table 1). The change

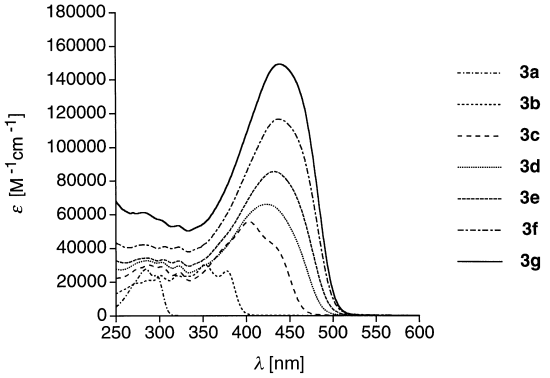

Figure 2. UV/Vis absorption spectra of PTA oligomers **3a–g** recorded in $CHCl_3$ at RT.

in $\Delta\lambda_{max}$ is 4 nm in going from hexameric **3d** to octameric **3e**, 3 nm from octameric **3e** to dodecameric **3f**, and from dodecameric **3f** to hexadecameric **3g** no additional increase in λ_{max} is observed. Direct determination of the ECL for optical absorption can be obtained by plotting the longest-wavelength absorption energy (E_{max}) versus the number of monomer units; this yields a value of about $n = 10$ repeating units, which is in accordance with the previous estimate of $n = 7–10$ monomer units (Figure 3).[14] A more elaborated

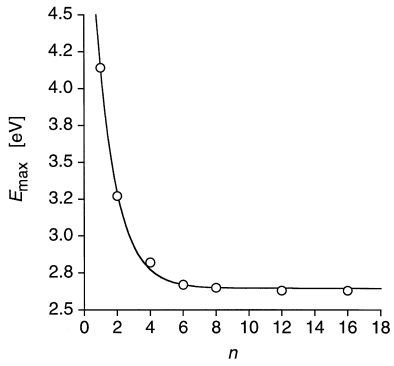

Figure 3. Plot of the deconvoluted longest-wavelength absorption energies E_{max} vs. the number of monomer units *n* with an overlaid exponential fit based on Equation (2).

determination of the ECL utilizing a "growth function" relationship between the absorption data and the number of repeating units *n* is given by the exponential Equations (1) and (2).[15]

$$\lambda_i(n) = \lambda_{i,\infty} + (\lambda_{i,\infty} - \lambda_{i,1})\, e^{-b_i(n-1)} \quad (1)$$

$$E_i(n) = E_{i,\infty} + (E_{i,1} - E_{i,\infty}) e^{-a_i(n-1)} \quad (2)$$

Herein, $\lambda_{i,1}$ and $E_{i,1}$ belong to the *i*-th absorption maxima, *n* corresponds to the number of monomer units, and $\lambda_{i,\infty}$ and

0947-6539/00/0619-3626 $ 17.50+.50/0 *Chem. Eur. J.* **2000**, *6*, No. 19

$E_{i,\infty}$ are the limiting values for an indefinitely long conjugated chain ($n \rightarrow \infty$). The differences $\Delta\lambda_i = \lambda_{i,\infty} - \lambda_{i,1}$ and $\Delta E_i = E_{i,1} - E_{i,\infty}$ represent the total shift of the absorption caused by the extension of the conjugation on going from a monomer ($n = 1$) to a polymer ($n = \infty$), and the parameters a_i and b_i, respectively, represent an indicator of how fast the limit of convergence is attained. It is important to note that the use of such an exponential "growth function" relationship lacks, at least at the moment, any theoretical background. The two exponential Equations are simply useful to fit the experimentally observed data in the most optimal way and their application is especially helpful in situations, where the oligomer data already display convergence and therefore a linear extrapolation to infinite chain length would result in misleading or even wrong conclusions. In order to allow the calculation of an ECL a "saturation criterion" has to be defined, which for practical reasons usually is based on the accuracy of an ordinary spectrophotometer with a typical resolution of ≥ 1 nm. This means that the maximum conjugation is virtually reached for n_{ECL}; any further increase of $\Delta\lambda_{max}$ between subsequent oligomers has to be smaller than 1 nm. For Equation (1) this yields to:

$$\lambda_{i,\infty} - \lambda_{i,ECL} \geq 1 \quad (3)$$

Applying an analogous criterion to Equation (2) using energy values, both Equations (1) and (2) reveal for the PTA oligomer series **3a–g** $n_{ECL} = 10$ with $\lambda_\infty = 471.2 \pm 1.3$ nm, $\Delta\lambda = 300.5 \pm 2.1$ nm, $b = 0.594 \pm 0.022$, and $E_\infty = 2.65 \pm 0.02$ eV, $\Delta E = 4.13 \pm 0.03$ eV, $a = 0.8216 \pm 0.052$, respectively. The saturation of linear optical properties has also been observed experimentally for dialkoxy-substituted oligo(*p*-phenylene vinylene)s,[15, 32] oligo(*p*-phenylene ethynylene)s,[23] oligo(α-thiophene ethynylene)s,[18, 19] *N*-methyl substituted pyrroles,[20] and oligo(9,10-anthrylene vinylene)s.[21] The parameter $b = 0.594$ for the PTA series, which characterizes the "velocity of convergence", is similar to that found for other π-conjugated systems. For instance, oligo(*p*-phenylene)s, oligo(*p*-phenylene vinylene)s, and oligo(α-thiophene ethynylene)s display comparable values to PTA oligomers with $b =$ 0.679, 0.574, and 0.535, respectively, whereas oligo(*p*-phenylene ethynylene)s exhibit the fastest saturation behavior among all the investigated systems with $b = 1.086$.[15]

The solution optical band gaps E_g of dodecamer **3f** and hexadecamer **3g** were determined at the intersection between the tangent passing through the turning point of the shoulder of the lowest-energy absorption band and the *x* axis. Both oligomers furnished with $E_g = 2.48$ eV (500 nm) a band gap validating the previously reported value of 2.4 eV (517 nm) for the polydisperse PTA polymer **2b**.[24] Interestingly, this value compares very well with $E_g = 2.48$ eV found for poly[2-methoxy-5-(2′-ethylhexyloxy)-*p*-phenylene vinylene] (MEH-PPV),[33] which has been widely investigated as the emissive material in electroluminescent devices. One of the most attractive features of PPVs are their excellent photo- and electroluminescent properties, which has made them an attractive class of polymers for use in light-emitting devices (PLEDs).[3, 34] In the case of PTAs, only relatively short oligomers such as dimeric **1b** and **3b** or trimeric **1c** display weak fluorescence ($\Phi_F = 0.01$).[35] Interestingly, going to higher chain lengths results in quenching of the fluorescence, a phenomenon which has also been observed in other π-conjugated systems such as oligo(α-thiophene)s.[36] In the latter case, this behavior has been rationalized on the basis of correlated semiempirical Hartree–Fock calculations in terms of the efficiency of intersystem-crossing processes between the singlet and triplet manifolds;[37] such a process is not likely to occur in the case of PTA chains due to the absence of heavy atoms within the conjugated backbone. Another explanation to rationalize the chain-size evolution of the luminescence properties is a possible cross-over in the relative positions of the $2A_g$ and $1B_u$ excited states when the chain length is increased.[38] The quenching of the luminescence would then result from the fact that the optically forbidden $2A_g$ state becomes the lowest in energy in high oligomers. The theoretical estimate of the relative position of the $2A_g$ versus $1B_u$ excited states in PTA oligomers is a hard computational task since this requires size-consistent highly correlated theoretical calculations going much beyond the INDO/SCI formalism. This was successfully achieved for oligoenes by using the density matrix renormalization group (DMRG) technique coupled to the PPP Hamiltonian.[38] Unfortunately, such an approach cannot yet treat the π-electrons lying in the plane of the molecule which play a critical role in determining the optical properties of the PTA chains.

Analysis of the optical properties of PTA monomers bearing different silyl end groups with the free diethynylethene derivative **4** indicates a strong dπ–pπ conjugative interaction between the terminal silicon atoms and the π-conjugated backbone. For example, the most intense electronic transition of the Me_3Si-end-capped monomer **1a** at 283 nm evolves to a value of 284 nm ($\Delta E = 0.02$ eV) for the Et_3Si-monomer **3b** and experiences a further red-shift to 286 nm ($\Delta E = 0.05$ eV) for the correspondent PTA monomer exhibiting $(i\text{Pr})_3Si$ end groups, which is a direct consequence of the increasing donor strength (inductive effect) of the alkyl groups attached to the silicon atoms.[39] Removal of both terminal silicon groups yielding the free diethynyl compound **4** results in a significant hypsochromic shift down to 262 nm, which clearly demonstrates the active participation of the silicon atoms in the π-conjugation. Similarly, the bis-silylated compound **1b** undergoes a shift of the lowest energy absorption band from 376 nm to 360 nm ($\Delta E = 0.15$ eV) upon cleavage to the free diethynyl dimer **6b**.[40, 41]

Nonlinear optical properties of the PTA oligomers: The third-order nonlinear optical properties of PTA oligomers **3a–g** were examined by third-harmonic generation (THG) and degenerate four-wave mixing (DFWM, Table 3).[42] The two methods provide values of the second-order hyperpolarizability γ located at different positions in the wavelength dispersion. Whereas THG delivers $\gamma(-3\omega,\omega,\omega,\omega)$, DFWM measurements give access to $\gamma(-\omega,\omega,-\omega,\omega)$ as the experimentally observed nonlinearity. As a result of the degenerate frequencies in the DFWM measurements, vibrational contributions can supplement the pure electronic contribution measured by THG.

Table 3. Second-order hyperpolarizabilities γ of Et_3Si-end-capped PTA oligomers **3a–g** and polymer **2a** measured by DFWM and THG[a] and theoretically calculated values.

Compound	n	γ_{DFWM} (10^{-36} esu)	γ_{DFWM} (10^{-48} m^5 V^{-2})	γ_{THG} (10^{-36} esu)	γ_{THG} (10^{-48} m^5 V^{-2})	$\gamma_{VEH/SOS}$ (10^{-36} esu)
3a	1	9	0.13	12	0.16	0.5
3b	2	77	1.1	54	0.75	33
3c	4	583	8.2	360	5.0	584
3d	6	1130	16	890	12	1878
3e	8	2180	31	1810	25	3497
3f	12	3530	49	2570	36	6892
3g	16	4290	60	4230	59	10315
2a	≈22	7530	105	6510	91	–

[a] Experimental error ± 10%.

The wavelengths of the incident laser beams are selected in such a way that no absorption of the fundamental or harmonic wavelengths occurs, thus guaranteeing a nonlinearity in the transparency range. As an additional verification of the nonresonant nonlinearity, temporal scans have been performed in the DFWM experiments, showing the instantaneous character of the measured hyperpolarizability and the absence of long-lived signal contributions from excited states.

The results for PTA oligomers **3a–g** and the two polydisperse polymer samples **2a**,**b** from THG and DFWM experiments disclose a power law increase $\gamma \cdot \alpha \cdot n^a$ of the hyperpolarizability γ for short oligomers, with a smooth saturation around $n = 10$ monomer units. The same qualitative result of $n = 10$ is obtained by plotting the nonlinearity per volume γ/n against the number of monomer units as shown in Figure 4. The power law exponent a for DFWM was

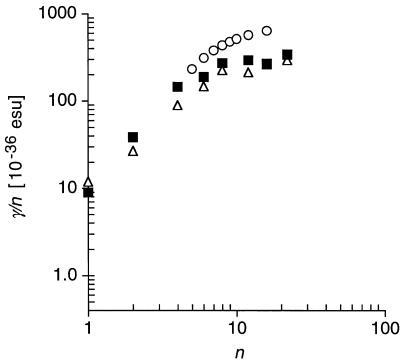

Figure 4. Double logarithmic plot of the second-order hyperpolarizability γ per monomer unit of PTA oligomers **3a–g** and polymer **2a** vs. the number of monomer units n measured by THG (△) and DFWM (■) together with the VEH/SOS calculated values (○). For short oligomers, the nonlinearity follows a power law $\gamma \cdot \alpha \cdot n^a$. Around 10 monomer units, the power law evolves smoothly into a linear increase; the onset of saturation of the nonlinearity per monomer unit γ/n is reached.

determined to 2.64 ± 0.20 for oligomers ranging up to octameric **3e**. The THG experiments revealed an exponent of $a = 2.46 \pm 0.10$, which corroborates well with $a = 2.52 \pm 0.10$ previously reported for series **1a–f**.[14]

The onset of saturation observed for the nonlinear optical properties takes place around 10 monomer units or 60 C–C bonds, which typically corresponds to the effective conjugation length determined from linear absorption data and electrochemical potentials. However, we should keep in mind that linear, nonlinear optical, and electrochemical measurements involve different physical processes and thus the three experimental characterizations should not reveal saturation a priori at the same chain length; direct comparisons between the three sets of experimental results have thus to be made with care. The power law dependence of the optical nonlinearity upon elongation of the π-conjugated backbone, yielding for PTAs an exponent a on the order of typically 2.5 and a saturation around 60 C–C bonds in the transparency range, has also been reported for other molecular systems.[42] We can therefore speculate that most linearly π-conjugated polymers follow a common law for the evolution of their nonlinear optical response upon lengthening of the backbone.

Theoretical calculations: The main goal of this theoretical section is to investigate the chain-length evolution of the electronic and optical properties of PTA oligomers and to assess the fundamental differences with respect to the properties of PAs and PDAs of similar size. We have first validated the use of the AM1 Hamiltonian to optimize the geometry of the entire PTA oligomer series by comparison of the C–C bond lengths calculated at the AM1 level for dimeric **3b** (excluding substituents) to those obtained from ab initio Hartree-Fock 6-31G* and post Hartree–Fock 6-31G*/MP2 (Möller–Plesset 2) calculations (Table 4). We observe very

Table 4. Characteristic C–C bond lengths (in Å) for PTA dimer **3b** bearing terminal hydrogen atoms instead of Et_3Si groups calculated on the AM1, ab initio 6–31G*, and 6–31G*/MP2 level of theory, together with corresponding experimental values obtained from X-ray single crystal structure analysis of PTA monomer **3a**.[14]

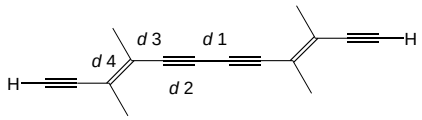

Bond	AM1	HF/6–31G*	MP2/6–31G*	Exp.
$d1$	1.349	1.383	1.360	–
$d2$	1.203	1.193	1.237	1.162
$d3$	1.399	1.431	1.413	1.425
$d4$	1.349	1.329	1.359	1.349

good correspondence between the AM1 and 6-31G*/MP2 results, which both indicate that the "single bond" located between two triple bonds has almost the same length as the double bond of the vinylene unit; noteworthy, this behavior is not reproduced at the 6-31G* level. The calculated bond lengths are also in good agreement with corresponding experimental values obtained from X-ray single crystal structure analysis experiments of monomeric **1a**;[14] the small discrepancies between the theoretical and experimental data

0947-6539/00/0619-3628 $ 17.50+.50/0 *Chem. Eur. J.* **2000**, *6*, No. 19

can be partly attributed to finite-size effects affecting the geometry of the monomer. The AM1-calculated C–C bond lengths in a PTA oligomer containing three repeat units together with the values obtained for PA and PDA chains with the same number of C atoms are reported in Figure 5. The

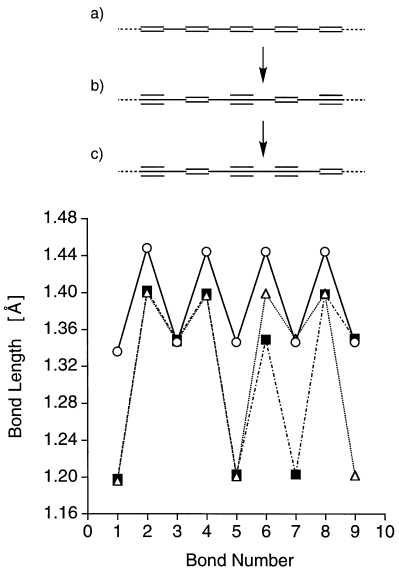

Figure 5. Evolution of the AM1-calculated C–C bond lengths [Å] going from a polyene a) containing 30 C atoms to PDA b) and PTA c) chains of similar size. The open circles, open triangles, and filled squares refer to the C–C bonds calculated for the polyene, PDA, and PTA backbones, respectively; for symmetry reasons, the C–C bond lengths calculated for one half of the molecule are represented on the graph. The arrow illustrates the significant reduction in the length of single C–C bonds when they become surrounded by triple bonds.

introduction of triple bonds along the conjugated backbone causes a reduction in the length of adjacent C–C single bonds and a simultaneous decrease in C–C bond alternation (i.e., increase in the cumulenic character) of the vinylene moieties, which is in agreement with earlier theoretical works;[43] the shortening of the single C–C bonds gets more pronounced when they are located between two triple bonds, as shown in Figure 5. The length of the PTA repeat unit is estimated to be 7.4 Å at the AM1 level and is similar to the value obtained from previous Molecular Mechanics (MM) calculations.[14, 22] The average C–C bond alternation (defined as the average of the absolute difference between two adjacent C–C bond lengths) is estimated to be 0.100 Å, 0.124 Å, and 0.129 Å for the PA, PDA, and PTA oligomers, respectively.

The evolution of the INDO-calculated gas-phase ionization potential and electron affinity of PTA oligomers (estimated within Koopmans' theorem as the absolute value of the HOMO and LUMO levels energy, respectively) as a function of the inverse number of repeat units is shown in Figure 6. For short oligomers (n between 2 and 7), the electron affinity increases with chain length; the linear relationship between electron affinity and inverse chain length parallels that obtained for the experimental formal redox potentials reported in Table 2 (slopes of 1.43 and 1.21 are obtained for the theoretical and experimental data, respectively). Deviation

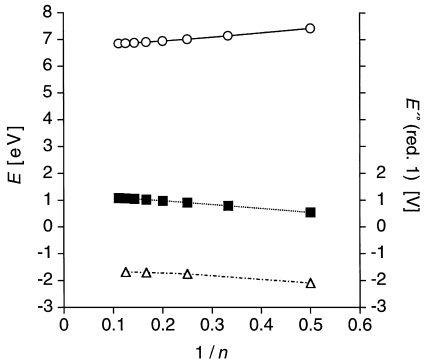

Figure 6. Evolution of the INDO-calculated gas-phase ionization potential (○) and electron affinity (■) of PTA chains as a function of the inverse number of repeat units. For comparison, the experimental reduction potentials [V] (△) taken from Table 2 are included.

from linear relationship is observed for longer chains, thus indicating that the onset of saturation of the electron affinity occurs around $n = 8$, which is in agreement with experimental values. Interestingly, the increase in electron affinity in going from one oligomer to the next has nearly the same amplitude as the decrease in ionization potential. This points to what condensed-matter physicists would refer to as a strong electron-hole symmetry in PTA chains. This symmetry is maximized when all the C atoms acquire very similar electronic characters and is thus supported by the experimental ^{13}C NMR results showing such a behavior.

The INDO/SCI-calculated energy of the lowest optically-allowed transition in PTA chains (for n varied between 1 and 6) is presented in Figure 7a. The CI expansion takes into account: i) only the molecular levels built from p_z atomic orbitals (denoted π_z in the following); and ii) the π_z molecular orbitals together with the π-type orbitals lying in the plane of the molecule (referred to as π_y levels, hereafter). In all cases, the transition originates from a mixing of both $\pi_z \rightarrow \pi_z^*$ and $\pi_y \rightarrow \pi_y^*$ one-electron excitations, which have the same symmetry within the C_{2h} representation applicable to the PTA oligomers. The neglect of the π_y levels in the CI leads to dramatic deviations with respect to the calculations performed with both π_z and π_y orbitals; this feature had already been emphasized in earlier calculations of Dinur and Karplus carried out on PDA oligomers.[44] The contribution arising from the $\pi_y \rightarrow \pi_y^*$ transitions is reduced as the chains elongate and leads to a progressive attenuation of the energy difference between the two sets of results. This is driven by the fact that the energies of the highest occupied and lowest unoccupied π_z orbitals significantly evolve with chain size due to the delocalization of the conjugated backbone, thus enlarging the energy gap (and decreasing the strength of the interaction) between them and the π_y orbitals (which are much less affected by the elongation of the chains). The calculated optical transitions overestimate by some 0.1–0.2 eV the experimental energies at the maximum of the lowest-energy absorption band in PTA chains ranging in size from 2 to 6 repeat units. Interestingly, a blue-shift on the order of 0.15 eV is also observed between the INDO/SCI-calculated and experimental spectra (in cyclohexane solution) of fullerene derivatives;[45] this shift is partly attributed to the

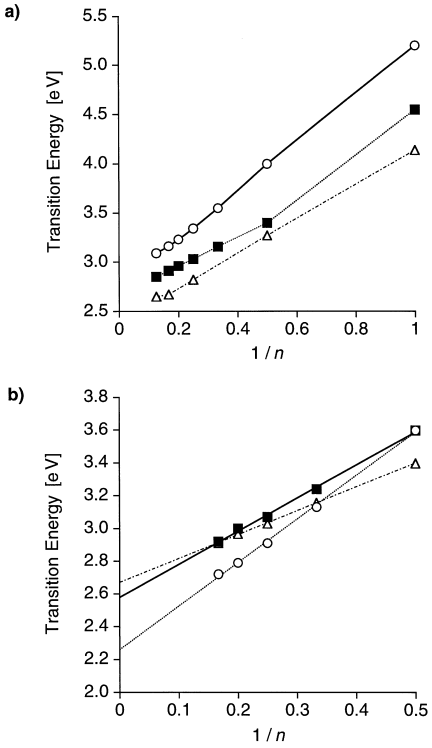

Figure 7. a) INDO/SCI-calculated evolution of the lowest optically allowed excited state of PTA chains as a function of the inverse number of monomer units n, as calculated with only π_z orbitals (○) and with both π_z and π_y orbitals (■); we also include the experimental deconvoluted absorption energies E_{max} for the PTA oligomers **3a–e** (△); b) INDO/SCI-calculated chain-size evolution of the lowest optically-allowed transition energy in PTA oligomers containing from 2 to 8 repeat units (△), together with the corresponding values obtained for PA (○) and PDA oligomers (■) possessing the same number of C atoms.

neglect of intra- and inter-chain polarization effects in the calculations. A linear relationship is observed between inverse chain length and the calculated transition energies for n varied between 2 and 8, in contrast to the experimental data showing the onset of saturation beyond 6 monomeric units. An interesting feature of PTA and PDA oligomers is that forbidden optical transitions are calculated to take place between π_z and π_y orbitals in an energy range very close to that of the lowest optically-allowed transition; such states can thus also play a critical role in determining the fluorescence properties of the chains.

The chain-size evolution of the INDO/SCI-calculated energy of the lowest optically-allowed transition in PTA oligomers (containing 12, 18, 24, 30, and 36 C atoms) together with the corresponding values obtained for PA and PDA oligomers having the same number of C atoms (note that the PDA oligomers with 18 and 30 C atoms have an extra double C–C bond) are reported in Figure 7b. We have estimated the band gap of the parent polymers from a linear regression through the oligomeric data extrapolated to the scale of an infinite chain ($n=\infty$); this procedure yields band gap values of 2.26 eV, 2.57 eV, and 2.67 eV for PA, PDA, and PTA, respectively. The evolution of the band gap energy can be correlated with the increase in average C–C bond alternation. Despite the fact that these results overestimate the experimental band gaps due to the neglect of polarization effects, they clearly demonstrate that PA has a significantly lower optical band gap than the other two polymers; a relevant comparison with experimental energies at λ_{max} measured for the three polymers is, however, not straightforward owing to the absence of experimental data acquired under similar conditions.[46] We also notice that the slope of the linear fit (2.66, 2.02, and 1.46 for PA, PDA, and PTA, respectively) decreases with the amount of triple bonds incorporated along the backbone; the slower evolution in PDA and PTA oligomers is thus consistent with triple bonds reducing the amplitude of delocalization effects associated to the photogenerated electron-hole pair (i.e., exciton). This is supported by a wavefunction analysis of the lowest optically allowed excited state in PA and PTA oligomers containing 30 C atoms, as shown in Figure 8. In such a two-dimensional graph, bright

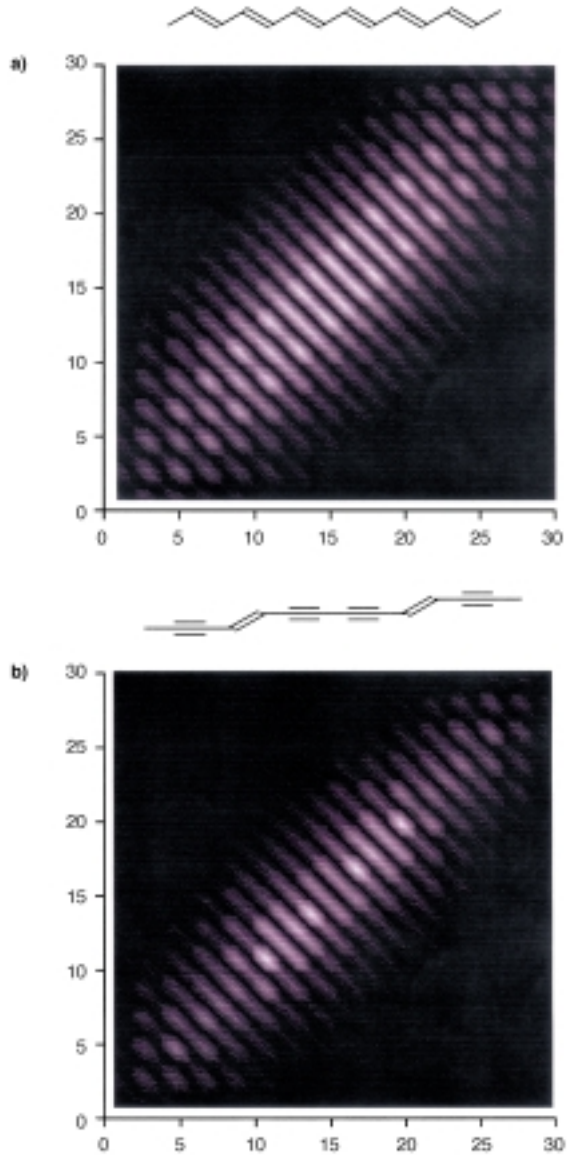

Figure 8. Representation of the electronic wavefunction of the electron-hole pair photogenerated in the lowest optically-allowed excited state of a PA a) and PTA b) chain containing 30 C atoms. Each data point (x_i,y_j) on the two-dimensional grid, running over all the C atoms along the x and y axes, is associated to the probability $|\psi(x_i,y_j)|^2$ of finding the first carrier on site x_i and the second carrier on site y_j; the brightest regions refer to the highest probabilities.

0947-6539/00/0619-3630 $ 17.50+.50/0 *Chem. Eur. J.* **2000**, *6*, No. 19

regions refer to high probabilities of finding the two carriers at the positions defined by the grid. In both cases, the wavefunction analysis reveals that the probabilities are the largest along the diagonal where the two carriers are very close to each other. When fixing one of the two carriers on a given site along the x axis, the extent of the electronic wavefunction of the exciton can be inferred by estimating the width of the bright zone along the corresponding vertical line. Widths on the order of 30 Å and 20 Å are found in the central part of the polyene and PTA chains, respectively; these can be compared to a value on the order of 30 Å previously reported for poly(*p*-phenylene vinylene) chains.[47]

The chain-size evolutions of the static average γ values per monomer unit calculated at the VEH/SOS level for PA, PDA, and PTA chains (up to 60 C atoms) are displayed in Figure 9.

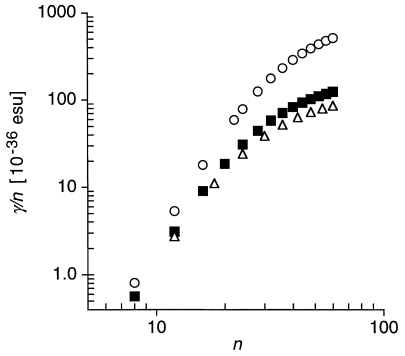

Figure 9. VEH/SOS-calculated evolution of the static γ values per monomer unit (in 10^{-36} esu) in PA (○), PDA (■), and PTA (△) chains as a function of the number of C atoms.

The third-order nonlinearities are much larger in polyenes than in chains of similar size containing triple C–C bonds. In accord with earlier correlated quantum-chemical calculations which addressed the way on how changes in the C–C bond alternation modulate the nonlinear optical properties in polyene-like derivatives,[48] this can be attributed to the increase in the C–C bond alternation in going from PA to PDA and PTA chains. The calculated evolutions fit a power law dependence $\gamma \cdot \alpha \cdot n^a$ for chains containing from 30 and 50 C atoms (i.e., in a range where the chains are expected to be well described by the VEH/SOS approach). The power law coefficients are estimated to be 2.34, 2.60, and 3.12 for the PTA, PDA, and PA chains, respectively, and can be correlated to changes in the strength of the interaction between the monomer units, as already suggested by the calculated linear optical properties. The static γ values obtained for longer chain lengths start to deviate from the power law, thus indicating the onset of a saturation regime. The theoretical power law coefficient a obtained for PTA chains (2.34) closely matches that estimated from THG and DFWM measurements (2.46 ± 0.10 and 2.64 ± 0.20, respectively).[42]

Conclusion

The fast and efficient statistical deprotection–oligomerization synthesis protocol presented in this work opens rapid access to monodisperse PTA oligomers with extended size. The entire PTA oligomer series featured amazingly high environmental stability combined with excellent solubilities in a wide range of aprotic organic solvents, thus enabling comprehensive structure–property studies by means of different characterization methods. The dodecamer and hexadecamer show a deviation from the typical linear chain-size evolution obtained for smaller π-conjugated oligomers, leading to a saturation in the first electrochemical reduction potential as well as in the linear and nonlinear optical properties. It is interesting to note that the effective conjugation length determined from the deconvoluted longest-wavelength absorptions is on the order of $n = 10$ monomeric units, in apparent agreement with the nonlinear optical measurements showing a smooth saturation of the second-order hyperpolarizability γ per monomer unit at approximately the same number of repeat units. All Et_3Si-end-capped PTA oligomers, except the hexadecamer, exhibited reversible one-electron transfer reduction events with saturation effects starting around the octamer. However, these data have to be interpreted with much caution since both cyclic and steady-state voltammetry give rise to poorly resolved peak potentials for the hexadecameric rod. Despite the different physical methods applied for the determination of the ECL, there is a striking accordance for the number of monomer units at which saturation effects become visible. However, since different physical effects govern the various characterization techniques that have been used, there is a priori no particular reason for which the electrochemical, Raman spectroscopical, linear optical, and nonlinear optical properties should lead to the same effective ECL; this issue will require further investigation.

The AM1 calculations indicate that introduction of triple bonds along the π-conjugated backbone of PTAs results in a reduction in the bond length of the adjacent C–C single bonds and a simultaneous decrease in C–C bond alternation of the vinylene moieties. INDO/SCI-calculated energies of the lowest optically-allowed transition revealed that the band gap is increased in the series PA, PDA, and PTA as a consequence of the introduction of the ethynylene bonds. The INDO-calculated gas-phase electron affinities obey a linear relationship as a function of the inverse number of monomer units, in agreement with the evolution of the reduction potentials found by electrochemical measurements. We have validated on the basis of VEH/SOS calculations the power law dependence between the second-order hyperpolarizability γ and the number of C atoms in PA, PDA, and PTA chains. The power law coefficient a estimated from both THG and DFWM experiments agrees very well with the theoretical value.

The analytical size-exclusion chromatography traces of oligomerized mixtures obtained from statistically deprotected **3e** indicate that even higher monodisperse PTA oligomers may be stable and isolable. Work along these directions aimed at synthesizing molecular rods of unprecedented length is currently pursued in our laboratory.

Experimental Section

Materials and general methods: Compound **4** was prepared as described in refs. [24, 25]. Reagents and solvents were purchased reagent-grade from Aldrich or Fluka and used without further purification. Anhydrous $MgSO_4$

was used as the drying agent after aqueous work-up. Evaporation and concentration in vacuo were carried out at water aspirator pressure. Column chromatography (CC): SiO_2 60 (70–270 mesh, 50–200 μm) from Macherey–Nagel, silica gel 60 (70–230 mesh, 63–200 μm) from Merck, or SiO_2 60 (230–400 mesh, 40–63 μm) from Fluka. Thin-layer chromatography (TLC): glass sheets covered with silica gel 60 F_{254} from Merck or Polygram SIL G/UV_{254} from Macherey–Nagel; visualization by UV light or dipping into a potassium permanganate solution and subsequent heating with a heat gun. Melting points (m.p.) were determined on a Büchi SMP-20 apparatus and are uncorrected. UV/Vis spectra were recorded on a Varian-Cary-5 spectrophotometer at RT. Infrared spectra were obtained on a Perkin–Elmer-1600-FT-IR spectrometer. Raman spectra were recorded on a Perkin–Elmer series 2000R NIR FT-Raman spectrometer. The compounds were excited in $CHCl_3$ solutions at 1064 nm (Nd:YAG laser, Spectron Laser Systems) at a laser power of 700–900 mW. ^{1}H- and ^{13}C-NMR spectra were recorded on a Bruker AMX-500 spectrometer; ^{13}C-NMR spectra with complete proton decoupling. Chemical shifts (δ) are reported in parts per million; residual protic solvent of $CHCl_3$ at $\delta = 7.24$ and the central resonance of the triplet for $CDCl_3$ at $\delta = 77.0$ were used as the internal reference in the ^{1}H- and ^{13}C-NMR spectra, respectively. The ^{13}C-NMR spectra of compounds **3e**, **3f**, and **3g** were recorded using $Cr(acac)_3$ ($\approx$20 mM) as a relaxation agent. For the monodisperse PTA oligomers **3b–g**, side chain atoms, in particular those belonging to the Me_2tBuSiOCH$_2$ side groups, frequently give rise to overlaps. However, in all cases apart from dodecamer and hexadecamer **3f** and **3g**, the unsaturated C atom resonances of the conjugated backbone were always clearly distinguishable. EI-MS spectra were acquired on a VG-Tribrid spectrometer measured at 70 eV. FAB-MS spectra were measured on a VG-ZAB-2SEQ spectrometer utilizing *m*-nitrobenzyl alcohol (3-NOBA) as the matrix. MALDI-TOF-MS spectra were obtained using a Bruker Reflex instrument with a N_2 laser system (337 nm) to desorb and ionize analyte molecules, which were previously dissolved in CH_2Cl_2 and deposited onto the center of the probe tip and dried under vacuum. 3-(3-Indolyl)acrylic acid (IAA), 2,5-dihydroxybenzoic acid (DHB), or 2′,4′,6′-trihydroxyacetophenone (THA)/ammonium hydrogencitrate (AHC) were used as matrices. All reported data were acquired using the linear positive-ion mode at +15 and 20 kV, respectively. For EI, FAB, and MALDI-TOF mass spectra, the experimental highest peak in the molecular ion cluster is reported followed in parenthesis by the isotopic molecular formula corresponding to the calculated most intense peak in the cluster. Elemental analyses were carried out by the Mikrolabor in the Laboratorium für Organische Chemie at ETH Zürich.

Analytical size-exclusion chromatography (SEC): Two columns connected in series: TosoHaas TSKgel G2500 HR (5 μm) and TosoHaas TSKgel G2000 HR (5 μm), 7.8 mm ID × 30 cm. Instrumentation: Merck-Hitachi HPLC pump L-7100; Merck–Hitachi column oven L-7360; Merck–Hitachi UV detector L-7400; Merck–Hitachi chromato-integrator D-2500; detector wavelength fixed at $\lambda = 400$ nm; solvent THF (HPLC grade) thermostatted at 60 °C with a flow rate fixed at 1 mL min^{-1}.

Preparative size-exclusion chromatography (SEC): Column: glass-column 5 × 180 cm, filled with Bio-Rad Bio-Beads S-X1. Instrumentation: UV/Vis detector from Knauer; all chromatograms recorded at ambient temperature with a variable detection wavelength ranging from $\lambda = 300$–600 nm; solvent: toluene or CH_2Cl_2 (technical grade, distilled prior to use) at RT; flow rate ca. 10 drops per min operated with gravity. The styrene/divinylbenzene copolymer gel was allowed to swell up for 24 h prior to use in approximately the seven-fold volume of solvent. Separation of hexadecamer **3g** was performed on a TosoHaas TSKgel G3000 HR (5 μm), 21.5 mm ID × 60 cm column. Instrumentation: Merck–Hitachi HPLC pump L-6250; Merck–Hitachi UV-detector L-4250; Merck–Hitachi refractive-detector; Merck–Hitachi chromato-integrator D-2500; detector wavelength fixed at $\lambda = 400$ nm; solvent: THF (HPLC grade) at RT; flow rate fixed at 5 mL min^{-1}.

Electrochemistry measurements: The electrochemical measurements were carried out at 20 ± 2 °C in CH_2Cl_2 containing 0.1 M nBu$_4$NPF$_6$ in a classical three-electrode cell. The electrochemical cell was connected to a computerized multipurpose electrochemical device (DACFAMOV, Microtec-CNRS, Toulouse, France) interfaced with an Apple II microcomputer. The working electrode was a glassy carbon disk electrode (∅ 2 mm, EDI-type, SOLEA-Tacussel, Villeurbanne, France) used either motionless for CV (10 mV s^{-1} to 10 V s^{-1}) or as a rotating-disk electrode. The auxiliary electrode was a Pt wire, and an aqueous Ag/AgCl electrode was used as reference electrode. All potentials are referenced to the ferrocene/ferricinium (Fc/Fc^+) couple which was used as an internal standard. The accessible range of potentials was +1.4 to −2.4 V versus Fc/Fc^+ on a glassy carbon electrode in CH_2Cl_2. CH_2Cl_2 was purchased spectroscopic grade from Merck, dried over 4 Å molecular sieves, and stored under Ar prior to use. nBu$_4$NPF$_6$ was purchased electrochemical grade from Fluka and used as received.

Third-harmonic generation measurements: The laser source was a pulsed Nd: YAG laser ($\lambda = 1.064$ μm, 10 Hz repetition rate, pulse duration of 5 ns) which was used to pump a H_2 gas Raman cell yielding a frequency shifted wavelength of $\lambda = 1.907$ μm. The *s*-polarized beam was focused onto the sample with a $f = 500$ mm lens. Third-harmonic generation measurements were performed by rotating the 1 mm thick fused silica cuvette with the solution parallel to the polarization to generate well known Maker-fringe interference patterns. The Maker-fringe patterns were analyzed in a manner similar to that described in the literature.[49] All measurements were calibrated against fused silica $\chi^{(3)}_{fs} = 1.62 \times 10^{-22}$ m^2 V^{-2} (1.16×10^{-14} esu).[50] A comparison of measurements of fused silica in vacuum and air allowed all subsequent measurements of our solutions to be performed in air. $CHCl_3$ solutions with initial concentrations of 0.5 to 1.5 weight percent were prepared and later diluted to four lower concentrations. From the concentration series the molecular second-order hyperpolarizability of the solute molecules was elucidated.

Degenerate four-wave mixing experiments: The laser source was a Nd: YLF laser ($\lambda = 1.047$ mm) with 10 ps pulses at a repetition rate of 10 Hz. Due to the short laser pulses, we can exclude thermal or orientational contributions of the solute molecule to the optical nonlinearity. The weak signal beam was detected with a pyroelectric joulemeter. The counter-propagating probe beam could be delayed in time to also measure the temporal behavior of the nonlinearity. All measurements were calibrated against CS_2 ($n_2 = 3.2 \times 10^{-5}$ GW cm^{-2}, $\chi^{(3)}_{fs} = 3.0 \times 10^{-20}$ m^2 V^{-2} $= 2.1 \times 10^{-12}$ esu).[51] $CHCl_3$ solutions of around 1 weight percent were prepared and diluted to four lower concentration. For each concentration two DFWM measurements were performed and the molecular second-order hyperpolarizability was calculated from the series.

Theoretical methodology: We have optimized the geometry of unsubstituted PTA oligomers ranging in size from $n = 1$ to 10 repeat units (i.e., from 6 to 60 C atoms) with the help of the semiempirical Hartree–Fock Austin Model 1 (AM1) method,[52] assuming planar conformations and the all-*trans* configuration indicated by the NMR and FT-IR experimental data. This choice of method is validated by the fact that AM1 has a very good track record for reproducing the ground-state geometry of organic molecules. For the sake of comparison, we have evaluated in the same way the equilibrium geometry of PA and PDA oligomers containing a similar number of C atoms.

On the basis of the structural data, we have computed the linear optical absorption properties of the oligomers by coupling the semiempirical intermediate neglect of differential overlap (INDO) Hamiltonian to a single configuration interaction scheme (SCI). We make use here of the INDO parameterization developed by Zerner and co-workers,[53] with the electronic interaction terms expressed by the Mataga–Nishimoto potential. In order to ensure size consistency, the singly excited configurations involved in the CI development are built from: i) all the occupied and unoccupied π-levels formed by a linear combination of p_z atomic orbitals that are perpendicular to the plane of the chain; ii) the $X/2$ highest occupied and $X/2$ lowest unoccupied levels that do not match the first criterion (with X being the total number of C atoms involved in triple C−C bonds); these molecular levels mostly originate from the C(sp) atoms and result from the interaction of π-atomic orbitals lying within the plane of the molecular backbone, which can also interact with the other valence atomic orbitals forming the σ-skeleton of the chain.

We have also characterized the nature of the electron-hole pair photogenerated in the lowest optically-allowed excited state of the chains by means of a wavefunction analysis carried out at the INDO/SCI level; this provides a two-dimensional grid running over all the C sites along each axis, where each data point (x,y) corresponds to the probability $|\psi(x_i,y_j)|^2$ of finding a charge carrier on site x and the second one on site y. Here, the amplitude $\psi(q,r)$ to have a carrier in orbital q (which can be a 2s, $2p_x$, $2p_y$, or $2p_z$ orbital) and the second carrier in orbital r is given by:

  0947-6539/00/0619-3632 $ 17.50+.50/0 *Chem. Eur. J.* **2000**, *6*, No. 19

$$\psi(q,r) = 1/\sqrt{2}[\sum^{j} C_j^{Cl} C_q^{LCAO}(e^-) C_r^{LCAO}(h^+) + \sum^{j} C_j^{Cl} C_q^{LCAO}(h^+) C_r^{LCAO}(e^-)] \quad (4)$$

where $C_q(h^+)$ and $C_r(e^-)$ are the LCAO (linear combination of atomic orbitals) coefficients in the occupied and unoccupied levels, respectively, involved in the *j*-th singly excited configuration. The orthonormalization of the basis set gives:

$$\sum^{q}\sum^{r} |\psi(q,r)|^2 = 1 \quad (5)$$

Regarding the third-order nonlinear optical properties, we have estimated the average static γ values of the chains with the help of the valence effective Hamiltonian (VEH)[54] method combined to a sum-over-states (SOS) formalism.[55] This approach has been shown to provide a reliable qualitative description of the third-order optical nonlinearities in long poly(acetylene) and poly(*p*-phenylene vinylene) chains.[56] The states plugged into the SOS expression of γ correspond to single Slater determinants obtained following single and double excitations between all the valence levels in oligomers containing up to 18 C atoms and between the 40 highest occupied and 40 lowest unoccupied molecular orbitals in longer chains.

(*E*)-3,4-Bis{[(*tert*-butyl)dimethylsilyloxy]methyl}-1-(triethylsilyl)hex-3-ene-1,5-diyne (5): 1.6 M *n*BuLi in *n*hexane (0.93 mL, 1.49 mmol) was added slowly to a solution of **4** (0.54 g, 1.49 mmol) in dry THF (40 mL) at −78 °C. After 30 min, Et_3SiCl (0.38 mL, 2.24 mmol) was added and the solution was warmed up to RT over a period of 1 h. Saturated aqueous NH_4Cl solution (50 mL) was added and the reaction mixture extracted with CH_2Cl_2 (200 mL). The organic phase was washed with saturated aqueous NaCl solution (100 mL) and dried ($MgSO_4$). Evaporation in vacuo and purification by CC (SiO_2 60, eluent: *n*hexane/CH_2Cl_2 3:1) gave **5** as a pale yellow oil (0.44 g, 66 %). ^{1}H NMR (200 MHz, $CDCl_3$): $\delta = 0.07$ (s, 12H), 0.66 (q, $J = 8.0$ Hz, 6H), 0.89 (s, 18H), 0.99 (t, $J = 8.0$ Hz, 9H), 3.49 (s, 1H), 4.42 (s, 2H), 4.47 (s, 2H); ^{13}C NMR (50 MHz, $CDCl_3$): $\delta = -5.31$, 4.22, 7.36, 18.31, 25.80, 63.86, 63.99, 80.43, 88.74, 102.49, 104.84, 129.85, 131.37; FT-IR ($CHCl_3$): $\tilde{\nu} = 3300$ (s), 2956 (s), 2929 (s), 2882 (s), 2860 (s), 2133 (m), 1600 (w), 1472 (s), 1462 (s), 1415 (m), 1390 (m), 1375 (m), 1362 (m), 1256 (s), 1167 (s), 1100 (s), 1039 (m), 1006 (m), 974 (w), 939 (w), 911 (m), 839 (s) cm^{-1}; EI-MS: *m*/*z* (%): 421.3 (1) $[M - C(CH_3)_3]^+$; $C_{26}H_{50}O_2Si_3$ (478.94): calcd C 65.20, H 10.52; found: C 65.17, H 10.65.

(*E*,*E*)-3,4,9,10-Tetrakis{[(*tert*-butyl)dimethylsilyloxy]methyl}-1,12-bis(triethylsilyl)dodeca-3,9-diene-1,5,7,11-tetrayne (3b): TMEDA (0.05 g, 0.07 mL, 0.44 mmol) and CuCl (0.012 g, 0.13 mmol) were added at RT to a solution of **5** (0.15 g, 0.32 mmol) in dry CH_2Cl_2 (20 mL, containing 4 Å molecular sieves). After stirring under an atmosphere of air for 5 h, an EDTA solution (pH 8, 100 mL) was added and the reaction mixture extracted with CH_2Cl_2 until the washings were colorless. The collected organic phases were washed with saturated aqueous NaCl solution (100 mL) and dried ($MgSO_4$). Removal of the solvent at reduced pressure and purification by a plug (SiO_2 60, eluent: *n*hexane/ethyl acetate 20:1) provided **3b** as a pale yellow solid (0.14 g, 97 %). M.p. 69–70 °C; ^{1}H NMR (500 MHz, $CDCl_3$): $\delta = 0.068$ (s, 12H), 0.073 (s, 12H), 0.62 (q, $J = 8.0$ Hz, 12H), 0.89 (s, 36H), 0.98 (t, $J = 8.0$ Hz, 18H), 4.40 (s, 4H), 4.48 (s, 4H); ^{13}C NMR (125.8 MHz, $CDCl_3$): $\delta = -5.22$, −5.16, 4.31, 7.45, 18.36, 18.38, 25.87, 25.91, 63.87, 64.07, 81.92, 85.47, 102.71, 107.07, 129.94, 132.95; FT-IR ($CHCl_3$): $\tilde{\nu} = 2956$ (s), 2929 (s), 2882 (s), 2856 (s), 2144 (m), 1567 (w), 1472 (s), 1462 (s), 1415 (m), 1390 (m), 1375 (m), 1361 (m), 1256 (s), 1172 (s), 1106 (s), 1006 (s), 972 (m), 911 (m), 839 (s) cm^{-1}; Raman ($CHCl_3$): $\tilde{\nu} = 3017$ (s), 2925 (w), 2399 (w), 2187 (w), 2132 (w), 1568 (w), 1498 (w), 1214 (m), 761 (m), 665 (s), 364 (s), 259 (s) cm^{-1}; UV/Vis ($CHCl_3$): $\lambda = 287$ (21200), 301 (24000), 320 (23800), 352 (30100), 377 (26500); FAB-MS: *m*/*z* (%): 954.5 (60) $[M]^+$, 897.4 (55) $[M - C(CH_3)_3]^+$, 823.3 (37) $[M - OSi(CH_3)_2C(CH_3)_3]^+$, 439.1 (100); MALDI-TOF-MS (THA, AHC): *m*/*z* (%): 977.9 (100) $[M+Na]^+$, 954.8 (36) $[M]^+$, 897.7 (46) $[M - C(CH_3)_3]^+$, 823.5 (95) $[M - OSi(CH_3)_2C(CH_3)_3]^+$; $C_{52}H_{98}O_4Si_6$ (955.87): calcd C 65.34, H 10.33; found: C 65.22, H 10.25.

Oligomers 3c and 3d: A 1 M NaOH solution (1 mL) was added at RT to a solution of **3b** (0.32 g, 0.33 mmol) in THF/CH_3OH (20 mL, 1:1), and the reaction was carefully monitored by TLC (*n*hexane/ethyl acetate 40:1). After the yellow spot of bis-deprotected **3b** appeared on the TLC (approximately 10 min), the reaction was immediately quenched by adding saturated aqueous NH_4Cl solution (100 mL) and extracted with CH_2Cl_2 (200 mL). The collected organic phases were dried ($MgSO_4$) and concentrated in vacuo to a volume of approximately 10 mL. The solution was diluted with dry CH_2Cl_2 (20 mL, containing 4 Å molecular sieves), and TMEDA (0.05 g, 0.07 mL, 0.46 mmol) and CuCl (0.012 g, 0.13 mmol) were added. After stirring under an atmosphere of air for 2 h at RT, an EDTA solution (pH 8, 100 mL) was added and the reaction mixture extracted with CH_2Cl_2 until the washings were colorless. The organic phase was washed with saturated aqueous NaCl solution (100 mL) and dried ($MgSO_4$). Concentration at water aspirator pressure, followed by purification using size-exclusion chromatography, and precipitation from MeOH gave the pure oligomers **3c** (0.057 g, 20 %) and **3d** (0.013 g, 5 %) besides recovered starting material **3b** (0.224 g, 70 %).

(*E*,*E*,*E*)-3,4,9,10,15,16,21,22-Octakis{[(*tert*-butyl)dimethylsilyloxy]methyl}-1,24-bis(triethylsilyl)tetracosa-3,9,15,21-tetraene-1,5,7,11,13,17,19,23-octayne (3c): Deep yellow solid; m.p. 151–152 °C; ^{1}H NMR (500 MHz, $CDCl_3$): $\delta = 0.069$ (s, 12H), 0.075 (s, 12H), 0.082 (s, 24H), 0.62 (q, $J = 8.0$ Hz, 12H), 0.890 (s, 36H), 0.894 (s, 36H), 0.99 (t, $J = 8.0$ Hz, 18H), 4.40 (s, 4H), 4.435 (s, 4H), 4.436 (s, 4H), 4.48 (s, 4H); ^{13}C NMR (125.8 MHz, $CDCl_3$): $\delta = -5.23$, −5.17, 4.29, 7.45, 18.35, 18.38, 25.86, 25.89, 63.84, 63.88, 64.07, 81.79, 83.13, 83.37, 85.22, 87.16, 87.61, 102.62, 107.47, 129.77, 132.03, 132.51, 133.33; FT-IR ($CHCl_3$): $\tilde{\nu} = 2956$ (m), 2932 (m), 2887 (w), 2856 (m), 2361 (w), 2339 (w), 2186 (w), 2131 (w), 1600 (m), 1472 (m), 1462 (m), 1411 (w), 1361 (w), 1256 (m), 1169 (w), 1106 (m), 1006 (m), 970 (w), 937 (w), 907 (w), 839 (s) cm^{-1}; Raman ($CHCl_3$): $\tilde{\nu} = 3017$ (m), 2925 (w), 2399 (w), 2169 (w), 2136 (w), 1558 (w), 1214 (m), 761 (m), 665 (s), 364 (s), 259 (s) cm^{-1}; UV/Vis ($CHCl_3$): $\lambda = 288$ (30000), 302 (29000), 323 (25800), 403 (55600), 425 (44300, sh); MALDI-TOF-MS (THA, AHC): *m*/*z* (%): 1702.5 (100) $[M+Na]^+$, 1680.5 (42) $[M]^+$, 1622.6 (79) $[M - C(CH_3)_3]^+$, 1548.8 (79) $[M - OSi(CH_3)_2C(CH_3)_3]^+$; $C_{92}H_{166}O_8Si_{10}$ (1681.20): calcd C 65.73, H 9.95; found: C 65.68, H 10.04.

(*E*,*E*,*E*,*E*,*E*)-3,4,9,10,15,16,21,22,27,28,33,34-Dodecakis{[(*tert*-butyl)dimethylsilyloxy]methyl}-1,36-bis(triethylsilyl)hexatriaconta-3,9,15,21,27,33-hexaene-1,5,7,11,13,17,19,23,25,29,31,35-dodecayne (3d): Deep yellow solid; m.p. 183–184 °C; ^{1}H NMR (500 MHz, $CDCl_3$): $\delta = 0.069$ (s, 12H), 0.075 (s, 12H), 0.083 (s, 48H), 0.62 (q, $J = 8.0$ Hz, 12H), 0.890 (s, 36H), 0.894 (s, 36H), 0.895 (s, 36H), 0.99 (t, $J = 8.0$ Hz, 18H), 4.40 (s, 4H), 4.44 (s, 16H), 4.48 (s, 4H); ^{13}C NMR (125.8 MHz, $CDCl_3$): $\delta = -5.23$, −5.17, 4.29, 7.46, 18.35, 18.38, 25.86, 25.90, 63.84, 63.89, 64.07, 81.77, 83.04, 83.21, 83.32, 83.42, 85.20, 87.09, 87.33, 87.43, 87.66, 102.61, 107.50, 129.76, 131.98, 132.31, 132.42, 132.60, 133.35; FT-IR ($CHCl_3$): $\tilde{\nu} = 2956$ (m), 2932 (m), 2887 (w), 2856 (m), 2398 (w), 2359 (w), 2340 (w), 2333 (w), 1600 (m), 1472 (m), 1462 (m), 1411 (w), 1361 (w), 1256 (m), 1170 (w), 1111 (m), 1006 (m), 979 (w), 941 (w), 911 (w), 839 (s) cm^{-1}; Raman ($CHCl_3$): $\tilde{\nu} = 3017$ (m), 2926 (w), 2399 (w), 2164 (w), 1556 (w), 1498 (w), 1214 (m), 761 (m), 665 (s), 364 (s), 259 (s) cm^{-1}; UV/Vis ($CHCl_3$): $\lambda = 285$ (32700), 303 (31700), 322 (29500), 423 (66000); MALDI-TOF-MS (THA, AHC): *m*/*z* (%): 2430.0 (100) $[M+Na]^+$, 2408.5 (68) $[M]^+$, 2350.0 (47) $[M - C(CH_3)_3]^+$, 2275.8 (68) $[M - OSi(CH_3)_2 - C(CH_3)_3]^+$; $C_{132}H_{234}O_{12}Si_{14}$ (2406.53): calcd C 65.88, H 9.80; found: C 65.84, H 9.83.

Oligomers 3e–g: A 1 M NaOH solution (1 mL) was added at RT to a solution of **3c** (0.10 g, 0.059 mmol) in THF/CH_3OH (30 mL, 1:1), and the reaction was carefully monitored by TLC (*n*hexane/ethyl acetate 40:1). After the yellow spot of bis-deprotected **3c** appeared on the TLC (approximately 10 min), the reaction was immediately quenched by adding saturated aqueous NH_4Cl solution (100 mL) and extracted with CH_2Cl_2 (200 mL). The collected organic phases were dried ($MgSO_4$) and concentrated in vacuo to a volume of approximately 10 mL. The solution was diluted with dry toluene (20 mL, containing 4 Å molecular sieves), and TMEDA (0.01 g, 0.01 mL, 0.083 mmol) and CuCl (0.002 g, 0.024 mmol) were added. The oligomerization was performed in refluxing toluene under an atmosphere of pure O_2. After 1 h, an EDTA solution (pH 8, 100 mL) was added and the mixture extracted with CH_2Cl_2 until the washings were colorless. The organic phase was washed with saturated aqueous NaCl solution (100 mL) and dried ($MgSO_4$). Concentration in vacuo, followed by purification using size-exclusion chromatography, and precipitation from MeOH gave the pure oligomers **3e** (0.018 g, 20 %), **3f** (0.009 g, 10 %), and **3g** (0.005 g, 5 %) besides recovered starting material **3c** (0.050 g, 50 %).

(*E*,*E*,*E*,*E*,*E*,*E*,*E*)-3,4,9,10,15,16,21,22,27,28,33,34,39,40,45,46-Hexadecakis{[(*tert*-butyl)dimethylsilyloxy]methyl}-1,48-bis(triethylsilyl)octatetraconta-3,9,15,21,27,33,39,45-octaene-1,5,7,11,13,17,19,23,25,29,31,35,37,41,43,

47-hexadecayne (3e): Deep yellow solid; m.p. 202–203 °C; ^{1}H NMR (500 MHz, $CDCl_3$): $\delta = 0.069$ (s, 12H), 0.075 (s, 12H), 0.083 (s, 72H), 0.62 (q, $J = 8.0$ Hz, 12H), 0.89 (s, 36H), 0.90 (s, 108H), 0.99 (t, $J = 8.0$ Hz, 18H), 4.40 (s, 4H), 4.44 (s, 24H), 4.48 (s, 4H); ^{13}C NMR (125.8 MHz, $CDCl_3$, $Cr(acac)_3$ added): $\delta = -5.35$, -5.29, 4.16, 7.33, 18.22, 18.25, 25.74, 25.77, 63.72, 63.76, 63.94, 81.64, 82.90, 83.06, 83.10, 83.13, 83.20, 83.29, 85.07, 86.95, 87.18, 87.23, 87.25, 87.32, 87.54, 102.49, 107.37, 129.63, 131.85, 132.17, 132.25, 132.27, 132.31, 132.48, 133.22; FT-IR ($CHCl_3$): $\tilde{\nu} = 3002$ (m), 2978 (s), 2900 (m), 2363 (w), 2338 (w), 1600 (w), 1482 (w), 1444 (m), 1394 (m), 1335 (w), 1305 (w), 1239 (m), 1044 (s), 938 (w), 878 (m), 805 (w) cm^{-1}; Raman ($CHCl_3$): $\tilde{\nu} = 3017$ (m), 2925 (w), 2399 (w), 2160 (w), 1553 (w), 1497 (w), 1214 (m), 761 (m), 666 (s), 364 (s), 259 (s) cm^{-1}; UV/Vis ($CHCl_3$): $\lambda = 286$ (34200), 304 (33300), 322 (32400), 432 (85600); MALDI-TOF-MS (THA, AHC): *m/z* (%): 3156.0 (100) $[M+Na]^+$, 3134.7 (30) $[M]^+$, 3075.3 (40) $[M - C(CH_3)_3]^+$, 3001.8 (43) $[M - OSi(CH_3)_2C(CH_3)_3]^+$; $C_{172}H_{302}O_{16}Si_{18}$ (3131.85): calcd C 65.96, H 9.72; found: C 65.76, H 9.89.

(*E*,*E*,*E*,*E*,*E*,*E*,*E*,*E*,*E*,*E*,*E*)-3,4,9,10,15,16,21,22,27,28,33,34,39,40,45,46,51,52,57,58,63,64,69,70-Tetracosakis{[(*tert*-butyl)dimethylsilyloxy]methyl}-1,72-bis(triethylsilyl)doheptaconta-3,9,15,21,27,33,39,45,51,57,63,69-dodecaene-1,5,7,11,13,17,19,23,25,29,31,35,37,41,43,47,49,53,55,59,61,65,67,71-tetracosayne (3f): Deep yellow solid; m.p. 219–220 °C; ^{1}H NMR (500 MHz, $CDCl_3$): $\delta = 0.069$ (s, 12H), 0.075 (s, 12H), 0.084 (s, 120H), 0.65 (q, $J =$ 8.0 Hz, 12H), 0.89 (s, 54H), 0.90 (overlap, 162H), 0.99 (t, $J = 8.0$ Hz, 18H), 4.40 (s, 4H), 4.44 (s, 40H), 4.48 (s, 4H); ^{13}C NMR (125.8 MHz, $CDCl_3$, $Cr(acac)_3$ added): $\delta = -5.51$ (overlap), 3.94, 7.12, 17.99 (overlap), 25.52 (overlap), 63.49 (overlap), 63.72 (overlap), 81.40, 83.06–82.66 (overlap, 10 signals), 84.84, 86.72, 87.01 (overlap, 7 signals), 87.09, 87.31, 102.25, 107.14, 129.40, 131.62, 131.94, 132.04 (overlap, 7 signals), 132.25, 132.99; FT-IR ($CHCl_3$): $\tilde{\nu} = 2956$ (s), 2927 (s), 2856 (s), 2188 (w), 2176 (w), 2132 (w), 2125 (w), 1600 (s), 1472 (s), 1460 (s), 1361 (m), 1256 (s), 1159 (w), 1111 (s), 1006 (m), 976 (w), 941 (w), 901 (w), 839 (s) cm^{-1}; Raman ($CHCl_3$): $\tilde{\nu} = 3017$ (m), 2925 (w), 2399 (w), 2158 (w), 1556 (w), 1496 (w), 1214 (m), 761 (m), 665 (s), 364 (s), 259 (s) cm^{-1}; UV/Vis ($CHCl_3$): $\lambda = 280$ (42100), 305 (41000), 322 (40800), 437 (116600); MALDI-TOF-MS (THA, AHC): *m/z* (%): 4604.9 (100) $[M+Na]^+$, 4581.9 (36) $[M]^+$, 4524.3 (40) $[M - C(CH_3)_3]^+$, 4450.7 (71) $[M - OSi(CH_3)_2C(CH_3)_3]^+$; $C_{252}H_{438}O_{24}Si_{26}$ (4582.51): calcd C 66.05, H 9.63; found: C 65.98, H 9.62.

(*E*,*E*,*E*,*E*,*E*,*E*,*E*,*E*,*E*,*E*,*E*,*E*,*E*,*E*,*E*)-3,4,9,10,15,16,21,22,27,28,33,34,39,40,45,46,51,52,57,58,63,64,69,70,75,76,81,82,87,88,93,94-Dotriacontakis{[(*tert*-butyl)dimethylsilyloxy]methyl}-1,96-bis(triethylsilyl)hexanonaconta-3,9,15,21,27,33,39,45,51,57,63,69,75,81,87,93-hexadecaene-1,5,7,11,13,17,19,23,25,29,31,35,37,41,43,47,49,53,55,59,61,65,67,71,73,77,79,83,85,89,91,95-dotriacontayne (3g): A 1M NaOH solution (1 mL) was added at RT to a solution of **3e** (0.10 g, 0.032 mmol) in THF/MeOH (90 mL, 1:1), and the reaction was carefully monitored by TLC (*n*hexane/ethyl acetate 20:1). After the yellow spot of bis-deprotected **3e** appeared on the TLC (approximately 10 min), the reaction was immediately quenched by adding saturated aqueous NH_4Cl solution (100 mL) and extracted with CH_2Cl_2 (200 mL). The collected organic phases were dried ($MgSO_4$) and concentrated in vacuo to a volume of approximately 10 mL. The solution was diluted with dry toluene (50 mL, containing 4 Å molecular sieves), and TMEDA (0.01 g, 0.01 mL, 0.045 mmol) and CuCl (0.001 g, 0.013 mmol) were added. The oligomerization was performed in refluxing toluene under an atmosphere of pure O_2. After 1 h, an EDTA solution (pH 8, 100 mL) was added and the reaction mixture extracted with CH_2Cl_2 until the washings were colorless. The organic phase was washed with saturated aqueous NaCl solution (100 mL) and dried ($MgSO_4$). Concentration at water aspirator pressure, followed by purification using size-exclusion chromatography, and precipitation from CH_3OH gave the pure oligomer **3g** (0.019 g, 20%), besides recovered starting material **3e** (0.070 g, 70%). Deep yellow solid; m.p. >220 °C; ^{1}H NMR (500 MHz, $CDCl_3$): $\delta = 0.069$ (s, 12H), 0.075 (s, 12H), 0.083 (s, 168H), 0.62 (q, $J = 7.9$ Hz, 12H), 0.89–0.90 (overlap, 288H), 0.99 (t, $J = 7.9$ Hz, 18H), 4.40 (s, 4H), 4.44 (s, 56H), 4.48 (s, 4H); ^{13}C NMR (125.8 MHz, $CDCl_3$, $Cr(acac)_3$ added): $\delta = -5.42$ (overlap), 4.03, 7.21, 18.09 (overlap), 25.60 (overlap), 63.59 (overlap), 63.81 (overlap), 81.52, 83.15–82.60 (overlap, 14 signals), 84.93, 86.81, 87.10 (overlap, 11 signals), 87.18, 87.40, 102.35, 107.25, 129.49, 132.19–131.69 (overlap, 13 signals), 132.35, 133.08; FT-IR ($CHCl_3$): $\tilde{\nu} = 2956$ (s), 2933 (s), 2856 (s), 2417 (w), 2383 (w), 2348 (w), 1667 (m), 1645 (m), 1600 (m), 1495 (m), 1461 (m), 1367 (m), 1261 (s), 1183 (m), 1168 (m), 1100 (s), 1072 (m), 1041 (m), 1017 (m), 922 (w), 839 (m), 811 (m) cm^{-1}; Raman ($CHCl_3$): $\tilde{\nu} = 3017$ (m), 2925 (w), 2398 (w), 2158 (w), 1555 (w), 1496 (w), 1214 (m), 761 (m), 665 (s), 364 (s), 259 (s) cm^{-1}; UV/Vis ($CHCl_3$): $\lambda = 270$ (61300), 281 (61200), 301 (56800, sh), 321 (53300), 439 (149400); MALDI-TOF-MS (IAA): *m/z* (%): 6055.6 (100) $[M+Na]^+$; $C_{332}H_{574}O_{32}Si_{34}$ (6033.16): calcd C 66.10, H 9.59; found: C 66.20, H 9.52.

(*E*,*E*)-3,4,9,10-Tetrakis{[(*tert*-butyl)dimethylsilyloxy]methyl}dodeca-3,9-diene-1,5,7,11-tetrayne (6b): K_2CO_3 (0.048 g, 0.34 mmol) was added slowly at RT to a solution of **3b** (0.10 g, 0.11 mmol) in THF/CH_3OH (10 mL, 1:1). After stirring for 30 min, the mixture was diluted with saturated aqueous NaCl (50 mL), extracted with CH_2Cl_2 (200 mL), and the organic phase dried ($MgSO_4$). Removal of the solvent at reduced pressure to a volume of about 10 mL and purification through a (short!) plug (silica gel 60, eluent: *n*hexane/ethyl acetate 10:1) provided **6b** (0.078 g, 98%). Attention: The compound is only stable in solution and must be stored under refrigeration at -20 °C! ^{1}H NMR (500 MHz, $CDCl_3$): $\delta = 0.129$ (s, 12H), 0.131 (s, 12H), 0.941 (s, 18H), 0.944 (s, 18H), 3.67 (s, 2H), 4.47 (s, 4H), 4.50 (s, 4H); ^{13}C NMR (125.8 MHz, $CDCl_3$): $\delta = -5.19$, -5.14, 18.35, 18.39, 25.88, 63.67, 64.02, 80.38, 81.54, 85.19, 90.64, 130.52, 132.23; FT-IR ($CHCl_3$): $\tilde{\nu} = 3303$ (s), 2968 (s), 2933 (s), 2894 (m), 2862 (s), 2246 (w), 1600 (w), 1472 (m), 1462 (m), 1440 (w), 1390 (w), 1364 (w), 1256 (s), 1215 (s), 1155 (m), 1103 (s), 1041 (w), 1005 (w), 841 (s) cm^{-1}; UV/Vis ($CHCl_3$): $\lambda = 264$ (19100), 277 (21400), 291 (21100), 311 (17600), 336 (23000), 360 (20800); FAB-MS: *m/z* (%): 726.3 (52) $[M]^+$, 669.3 (71) $[M - C(CH_3)_3]^+$, 595.3 (62) $[M - OSi(CH_3)_2C(CH_3)_3]^+$, 555.3 (100).

Acknowledgement

This work was supported by the ETH Research Council. We are grateful to Mr. Thomas Mäder for help with the purification of hexadecamer **3g** by preparative SEC and Mrs. Patrizia Fabrizoli for assistance with the Raman spectroscopy. The work in Mons is supported by the Belgian Federal Government (Pôle d'Attraction Interuniversitaire en Chimie Supramoléculaire et Catalyse, PAI 4/11) and the Belgian National Fund for Scientific Research (FNRS). J.C. is an FNRS research fellow.

[1] a) A. Rajca, *Chem. Rev.* **1994**, *94*, 871–893; b) J. S. Miller, A. J. Epstein, *Angew. Chem.* **1994**, *106*, 399–432; *Angew. Chem. Int. Ed. Engl.* **1994**, *33*, 385–415; c) J. S. Miller, *Adv. Mater.* **1992**, *4*, 435–438.

[2] a) *Handbook of Conducting Polymers* (Eds.: T. A. Skotheim, R. L. Elsenbaumer, J. R. Reynolds), 2nd ed., Marcel Dekker, New York **1998**; b) *Handbook of Organic Conductive Molecules and Polymers*, *Vol. 1–4* (Ed.: H. S. Nalwa), Wiley, Chichester, **1997**.

[3] a) F. Cacialli, *Curr. Opin. Coll. Int. Sci.* **1999**, *4*, 159–164; b) R. H. Friend, R. W. Gymer, A. B. Holmes, J. H. Burroughes, R. N. Marks, C. Taliani, D. D. C. Bradley, D. A. Dos Santos, J. L. Brédas, M. Lögdlund, W. R. Salaneck, *Nature* **1999**, *397*, 121–128; c) A. Kraft, A. C. Grimsdale, A. B. Holmes, *Angew. Chem.* **1998**, *110*, 416–443; *Angew. Chem. Int. Ed.* **1998**, *37*, 402–428; d) J. L. Segura, *Acta Polym.* **1998**, *49*, 319–344.

[4] a) M. Granström, K. Petritsch, A. C. Arias, A. Lux, M. R. Andersson, R. H. Friend, *Nature* **1998**, *395*, 257–260; b) K. Tada, M. Onoda, A. A. Zakhidov, K. Yoshino, *Jpn. J. Appl. Phys. Pt2-Lett.* **1997**, *36*, L306-L309; c) K. Takahashi, S. Nakatani, T. Yamaguchi, T. Komura, S. Ito, K. Murata, *Solar Energy Mater. Solar Cells* **1997**, *45*, 127–139; d) K. Yoshino, K. Tada, A. Fujii, E. M. Conwell, A. A. Zakhidov, *IEEE Trans. Electron. Devices* **1997**, *44*, 1315–1324; e) G. Yu, A. J. Heeger, *J. Appl. Phys.* **1995**, *78*, 4510–4515; f) J. J. M. Halls, C. A. Walsh, N. C. Greenham, E. A. Marseglia, R. H. Friend, S. C. Moratti, *Nature* **1995**, *376*, 498–500.

[5] a) G. Horowitz, *Adv. Mater.* **1998**, *10*, 365–377; b) H. E. Katz, J. G. Laquindanum, A. J. Lovinger, *Chem. Mater.* **1998**, *10*, 633–638; c) T. Siegrist, C. Kloc, R. A. Laudise, H. E. Katz, R. C. Haddon, *Adv. Mater.* **1998**, *10*, 379–382; d) G. Barbarella, P. Ostoja, P. Maccagnani, O. Pudova, L. Antolini, D. Casarini, A. Bongini, *Chem. Mater.* **1998**, *10*, 3683–3689; e) H. Sirringhaus, R. H. Friend, X. C. Li, S. C. Moratti, A. B. Holmes, N. Feeder, *Appl. Phys. Lett.* **1997**, *71*, 3871–3873; f) R. Hajlaoui, D. Fichou, G. Horowitz, B. Nessakh, M. Constant, F. Garnier, *Adv. Mater.* **1997**, *9*, 557–561; g) D. Fichou, M.-P. Teulade-Fichou, G. Horowitz, F. Demanze, *Adv. Mater.* **1997**, *9*, 75–80.

  0947-6539/00/0619-3634 $ 17.50+.50/0

[6] a) R. R. Tykwinski, U. Gubler, R. E. Martin, F. Diederich, C. Bosshard, P. Günter, *J. Phys. Chem. B* **1998**, *102*, 4451–4465; b) J. L. Brédas, C. Adant, P. Tackx, A. Persoons, B. M. Pierce, *Chem. Rev.* **1994**, *94*, 243–278; c) H. S. Nalwa in *Nonlinear Optics of Organic Molecules and Polymers* (Eds.: H. S. Nalwa, S. Miyata), CRC Press, New York, **1997**, pp. 611–798; d) S. R. Marder, B. Kippelen, A. K.-Y. Jen, N. Peyghambarian, *Nature* **1997**, *388*, 845–851; e) A. J. Heeger, J. Long, Jr., *Optics & Photonics News* **1996**, *7*, 24–30; f) For a recent overview on functional organic materials for electronic and optoelectronic devices, see special issues: *J. Mater. Chem.* **1999**, *9*, 1853–2276 and *Acc. Chem. Res.* **1999**, *32*, 191–276.

[7] R. H. Friend, J. Burroughes, T. Shimoda, *Physics World* **1999**, *12*, 35–40.

[8] *Electronic Materials*: *The Oligomer Approach* (Eds.: K. Müllen, G. Wegner), WILEY-VCH, Weinheim, **1997**.

[9] a) J. Roncali, *Chem. Rev.* **1997**, *97*, 173–205; b) J. M. Tour, *Chem. Rev.* **1996**, *96*, 537–553.

[10] a) D. Bloor in *Introduction to Molecular Electronics* (Eds.: M. C. Petty, M. R. Bryce, D. Bloor), Edward Arnold, London, **1995**, pp. 1–28; b) For an excellent overview on molecular electronics, see: *Molecular Electronics*: *Science and Technology*, *Vol. 852* (Eds.: A. Aviram, M. Ratner), The New York Academy of Sciences, New York, **1998**, and references therein.

[11] R. E. Martin, F. Diederich, *Angew. Chem.* **1999**, *111*, 1440–1469; *Angew. Chem. Int. Ed.* **1999**, *38*, 1350–1377.

[12] K. Müllen, *Pure Appl. Chem.* **1993**, *65*, 89–96.

[13] U. Scherf, K. Müllen, *Synthesis* **1992**, 23–38.

[14] R. E. Martin, U. Gubler, C. Boudon, V. Gramlich, C. Bosshard, J.-P. Gisselbrecht, P. Günter, M. Gross, F. Diederich, *Chem. Eur. J.* **1997**, *3*, 1505–1512.

[15] H. Meier, U. Stalmach, H. Kolshorn, *Acta Polymer.* **1997**, *48*, 379–384.

[16] a) G. Zerbi, E. Galbiati, M. C. Gallazi, C. Castiglioni, M. Del Zoppo, R. Schenk, K. Müllen, *J. Chem. Phys.* **1996**, *105*, 2509–2516; b) J. Grimme, M. Kreyenschmidt, F. Uckert, K. Müllen, U. Scherf, *Adv. Mater.* **1995**, *7*, 292–295; c) J. Guay, P. Kasai, A. Diaz, R. Wu, J. M. Tour, L. H. Dao, *Chem. Mater.* **1992**, *4*, 1097–1105; d) S. A. Jenekhe, *Macromolecules* **1990**, *23*, 2848–2854; e) J. L. Brédas, R. Silbey, D. S. Boudreaux, R. R. Chance, *J. Am. Chem. Soc.* **1983**, *105*, 6555–6559.

[17] a) G. Klaerner, R. D. Miller, *Macromolecules* **1998**, *31*, 2007–2009; b) W. Li, T. Maddux, L. Yu, *Macromolecules* **1996**, *29*, 7329–7334.

[18] D. L. Pearson, J. M. Tour, *J. Org. Chem.* **1997**, *62*, 1376–1387.

[19] D. L. Pearson, J. S. Schumm, J. M. Tour, *Macromolecules* **1994**, *27*, 2348–2350.

[20] T. Kauffmann, H. Lexy, *Chem. Ber.* **1981**, *114*, 3674–3683.

[21] H.-P. Weitzel, A. Bohnen, K. Müllen, *Makromol. Chem.* **1990**, *191*, 2815–2835.

[22] R. E. Martin, T. Mäder, F. Diederich, *Angew. Chem.* **1999**, *111*, 834–838; *Angew. Chem. Int. Ed.* **1999**, *38*, 817–821.

[23] For a 12.8 nm long hexadecamer with a poly(*p*-phenylene ethynylene) backbone, see: J. S. Schumm, D. L. Pearson, J. M. Tour, *Angew. Chem.* **1994**, *106*, 1445–1448; *Angew. Chem. Int. Ed. Engl.* **1994**, *33*, 1360–1363.

[24] M. Schreiber, J. Anthony, F. Diederich, M. E. Spahr, R. Nesper, M. Hubrich, F. Bommeli, L. Degiorgi, P. Wachter, P. Kaatz, C. Bosshard, P. Günter, M. Colussi, U. W. Suter, C. Boudon, J.-P. Gisselbrecht, M. Gross, *Adv. Mater.* **1994**, *6*, 786–790.

[25] J. Anthony, Ph. D. Thesis, University of California, Los Angeles, **1993**.

[26] R. E. Martin, J. Bartek, V. Gramlich, F. Diederich, R. R. Tykwinski, E. C. Meister, A. Hilger, H. P. Lüthi, *J. Chem. Soc. Perkin Trans. 2* **1998**, 233–241.

[27] a) A. M. Boldi, J. Anthony, C. B. Knobler, F. Diederich, *Angew. Chem.* **1992**, *104*, 1270–1273; *Angew. Chem. Int. Ed. Engl.* **1992**, *31*, 1240–1242; b) J. Anthony, C. Boudon, F. Diederich, J.-P. Gisselbrecht, V. Gramlich, M. Gross, M. Hobi, P. Seiler, *Angew. Chem.* **1994**, *106*, 794–798; *Angew. Chem. Int. Ed. Engl.* **1994**, *33*, 763–766; c) A. M. Boldi, J. Anthony, V. Gramlich, C. B. Knobler, C. Boudon, J.-P. Gisselbrecht, M. Gross, F. Diederich, *Helv. Chim. Acta* **1995**, *78*, 779–796.

[28] J. L. Brédas, J. Cornil, A. J. Heeger, *Adv. Mater.* **1996**, *8*, 447–452.

[29] P. Bäuerle, *Adv. Mater.* **1992**, *4*, 102–107.

[30] E. H. Elandaloussi, P. Frére, P. Richomme, J. Orduna, J. Garin, J. Roncali, *J. Am. Chem. Soc.* **1997**, *119*, 10774–10784.

[31] R. Schenk, H. Gregorius, K. Meerholz, J. Heinze, K. Müllen, *J. Am. Chem. Soc.* **1991**, *113*, 2634–2647.

[32] U. Stalmach, H. Kolshorn, I. Brehm, H. Meier, *Liebigs Ann.* **1996**, 1449–1456.

[33] D.-H. Hwang, B. S. Chuah, X.-C. Li, S. T. Kim, S. C. Moratti, A. B. Holmes, *Macromol. Symp.* **1997**, *125*, 111–120.

[34] D. D. C. Bradley, *Chem. Brit.* **1991**, 719–723.

[35] R. E. Martin, J. A. Wytko, F. Diederich, C. Boudon, J.-P. Gisselbrecht, M. Gross, *Helv. Chim. Acta* **1999**, *82*, 1470–1485.

[36] J. Cornil, D. Beljonne, J. L. Brédas in *Electronic Materials*: *The Oligomer Approach* (Eds.: K. Müllen, G. Wegner), WILEY-VCH, Weinheim, **1997**, pp. 432–447.

[37] D. Beljonne, J. Cornil, R. H. Friend, R. A. J. Janssen, J. L. Brédas, *J. Am. Chem. Soc.* **1996**, *118*, 6453–6461.

[38] Z. Shuai, J. L. Brédas, S. K. Pati, S. Ramasesha, *Proc. SPIE—Int. Soc. Opt. Eng.* **1997**, *3145*, 293–302.

[39] R. E. Martin, Dissertation, ETH Zürich, No. 12821, **1998**.

[40] *The Chemistry of Organic Silicon Compounds* (Eds.: S. Patai, Z. Rappoport), Wiley, Chichester, **1989**.

[41] J. M. Tour, R. Wu, *Macromolecules* **1992**, *25*, 1901–1907.

[42] U. Gubler, C. Bosshard, P. Günter, M. Y. Balakina, J. Cornil, J. L. Brédas, R. E. Martin, F. Diederich, *Opt. Lett.* **1999**, *24*, 1599–1601.

[43] J. L. Brédas, M. Dory, J. M. André, *J. Chem. Phys.* **1985**, *83*, 5242–5249.

[44] U. Dinur, M. Karplus, *Chem. Phys. Lett.* **1982**, *88*, 171–176.

[45] P. F. Coheur, J. Cornil, D. A. dos Santos, P. R. Birkett, J. Liévin, J. L. Brédas, D. R. M. Walton, R. Taylor, H. W. Kroto, R. Colin, unpublished results.

[46] In terms of conformational and environmental effects that can promote shifts in the absorption maxima larger than the calculated energy differences, see for instance: D. Comoretto, I. Moggio, C. Cuniberti, G. Dellepiane, M. E. Giardini, A. Borghesi, *Phys. Rev. B* **1997**, *56*, 10264–10270.

[47] J. L. Brédas, J. Cornil, D. Beljonne, D. A. dos Santos, Z. Shuai, *Acc. Chem. Res.* **1999**, *32*, 267–276.

[48] a) F. Meyers, S. R. Marder, B. M. Pierce, J. L. Brédas, *J. Am. Chem. Soc.* **1994**, *116*, 10703–10714; b) S. R. Marder, C. B. Gorman, F. Meyers, J. W. Perry, G. Bourhill, J.-L. Brédas, B. M. Pierce, *Science* **1994**, *265*, 632–635.

[49] F. Kajzar, J. Messier, *Phys. Rev. A* **1985**, *32*, 2352–2363.

[50] C. Bosshard in *Nonlinear Optical Effects and Materials* (Springer Series in Optical Sciences) (Ed.: P. Günter), Springer Verlag, Berlin, **1999**.

[51] M. Sheik-Bahae, A. A. Said, T.-H. Wei, D. J. Hagan, E. W. Van Stryland, *IEEE J. Quantum Electron.* **1990**, *26*, 760–769.

[52] M. J. S. Dewar, E. G. Zoebisch, E. F. Healy, J. J. P. Stewart, *J. Am. Chem. Soc.* **1985**, *107*, 3902–3909.

[53] J. Ridley, M. Zerner, *Theor. Chim. Acta* **1973**, *32*, 111–134.

[54] J. L. Brédas, R. R. Chance, R. Silbey, G. Nicolas, P. Durand, *J. Chem. Phys.* **1981**, *75*, 255–267.

[55] B. J. Orr, J. F. Ward, *Mol. Phys.* **1971**, *20*, 513–526.

[56] Z. Shuai, J. L. Brédas, *Phys. Rev. B* **1991**, *44*, 5962–5965.

Received: February 2, 2000 [F2271]